

A Very Impressive and Fancy Title for a Thesis

by

Giovanni Pederiva

THESIS

for the degree of

MASTER OF SCIENCE



Faculty of Mathematics and Natural Sciences
University of Oslo

May 2018

Contents

I	Introduction to QCD and Lattice Field Theories	5
1	A Primer on QCD in the Continuum	7
1.1	The QCD Lagrangian	8
1.1.1	Feynman Rules of QCD	9
1.1.2	Gauge Symmetry of the Lagrangian	10
1.2	General Properties of QCD	12
1.2.1	Running Coupling	12
1.3	Methods and Regimes of Chromodynamics	14
2	Lattice Field Theories and Lattice QCD	17
2.1	Discretizing Field Theories	17
2.1.1	The Harmonic Oscillator Example	18
2.2	Discretization of QCD on the Lattice	18
2.2.1	Naïve Discretization of Fermions	18
2.2.2	The Gauge Transporter and the Wilson Loop	19
2.2.3	Lattice Fermions	21
2.3	Path Integrals on the Lattice	21
2.3.1	Pure Gauge Field Theory	23
2.3.2	Observables	23

2.4	Modern Lattice QCD Calculations	25
3	Advanced Topics in Lattice QCD	27
3.1	Scale Setting in the Quenched Approximation	27
3.2	The Gradient Flow Method	28
3.3	Perturbative Analysis of the Wilson Flow	29
3.3.1	Scale Fixing with the Gradient Flow	30
3.4	Estimating the Scale Parameter	32
3.4.1	4-loop Corrected Running Coupling	32
II	Implementation	35
4	Designing a Lattice $SU(3)$ Yang-Mills Theory Code	37
4.1	Generating Pure Gauge Fields	37
4.1.1	The Metropolis Algorithm	38
4.1.2	Sampling the Configuration Space	39
4.1.3	Updates Strategies	41
4.1.4	Parallelization Scheme	41
4.1.5	Summary of the Parameters	42
4.2	Wilson Flow of Gauge Configurations	42
4.2.1	The Action Derivative	43
4.2.2	Exponential of a $\mathfrak{su}(3)$ Element	43
4.2.3	Parallelization Scheme	44
4.3	Structure and Tools	45
5	Tests and Runs Description	47
5.1	Generated Ensembles	47

5.2	Test Runs	48
5.2.1	Strong and Weak Scaling	48
5.2.2	Autocorrelation of Observables	49
5.3	Production Runs and Timing	49
 III Data Analysis and Results		51
6	Raw Observables	53
7	Running Coupling and Scale Fixing	55
 IV Conclusion and Discussion		57
8	Summary and Conclusion	59
9	Future Developements	61
 V Appendices		63

Abstract

some abstract

Acknowledgements

Part I

Introduction to QCD and Lattice Field Theories

Chapter 1

A Primer on QCD in the Continuum

The Standard Model of particle physics (SM) is the theory of fundamental particles and their interactions. Three of the four known fundamental forces are described by it, the exception is gravity, so all phenomena regarding the Electromagnetic, Weak and Strong forces are included within the theory. The SM describes quantized fields defined on all space-time whose excitations are commonly identified with particles. There are two categories of particles, depending on the spin statistic they can be: fermions, quarks or leptons in the SM, which are the constituents of matter; or bosons, which mediate the interactions between particles.

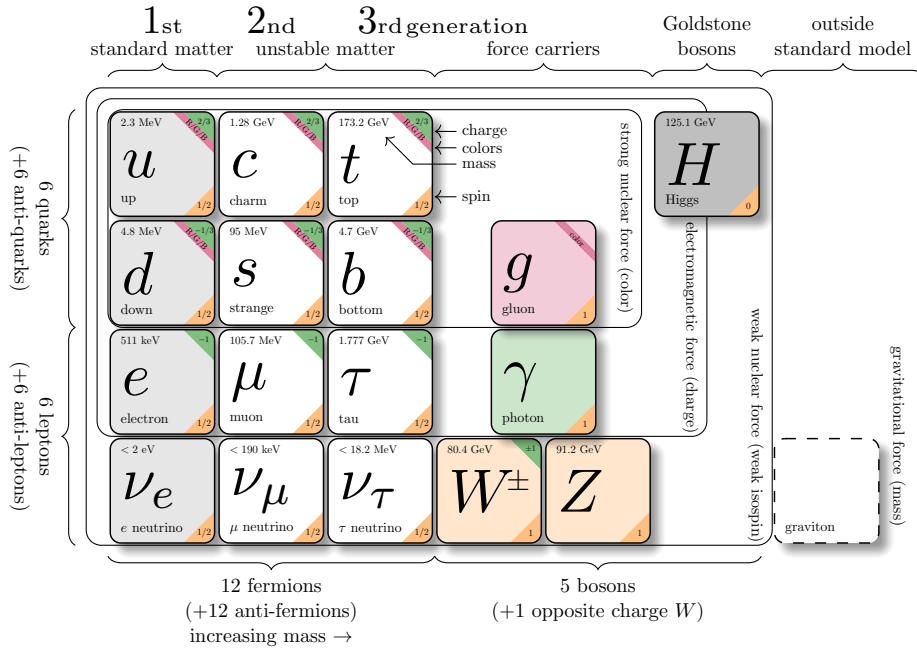


Figure 1.1: Summary of the particles on the Standard Model [1]

From a group theory point of view, the SM is the composition of three different local gauge symmetry groups, each associated with a fundamental force:

$$SU(3)_C \times \underbrace{SU(2)_L \times U(1)_Y}_{\text{broken to } SU(2)_W \times U(1)_Q} \quad (1.1)$$

The $U(1)_Q$ symmetry group is associated with the electromagnetic interaction and $SU(2)_W$ is the weak interaction. They both derive from the spontaneously broken, through the Higgs mechanism, symmetry $SU(2)_L \times U(1)_Y$ that defines the unified electroweak theory.

Quantum Chromodynamics, commonly referred to as QCD, is the quantum field theory, contained in the SM, that describes the behavior of strongly interacting matter, that is quarks and gluons. It is a non-abelian gauge theory based on a $SU(3)$ symmetry group. The associated quantum number is called “color charge” which pictorially can assume the values of *red* (r), *green* (g), *blue* (b), *anti-red* (\bar{r}), *anti-green* (\bar{g}) or *anti-blue* (\bar{b}). In this chapter we will discuss the QCD lagrangian density, its properties and some of the major results of the theory. Some intermediate knowledge of Quantum Field Theory is assumed and derivations and proofs mainly follow the reasoning found in [2].

1.1 The QCD Lagrangian

In Quantum Field Theory (QFT) the characterizing equation of a theory is its *lagrangian density*, because it contains all the information about the fields that are involved, their properties and most importantly, their interactions. For QCD the simplest form is based on the Yang-Mills Lagrangian, with a $SU(3)$ local gauge symmetry group:

$$\mathcal{L}_{QCD} = -\frac{1}{4}(G_{\mu\nu}^a)^2 + \sum_{f=1}^{N_f} \bar{\psi}_f(i\not{D} - m_f)\psi_f \quad (1.2)$$

Here ψ_f represents the complex-valued fermion field of flavor f , with mass m_f . These are associated with the quark fields and come in six flavors: u (up), d (down), s (strange), c (charm), b (bottom) and t (top). The second element in the lagrangian is the Gluon Field Strength Tensor, $G_{\mu\nu}^a$. The two indices μ and ν are Lorentz indices and a is the index of the generators of the gauge group, $SU(3)$ in this case. Note that Einstein summing convention on repeated indices is implicit, for example when taking the square of the field strength tensor three sums are applied. The definition of $G_{\mu\nu}^a$ is:

$$G_{\mu\nu}^a = \partial_\mu A_\nu^a - \partial_\nu A_\mu^a + g_0 f^{abc} A_\mu^b A_\nu^c \quad (1.3)$$

in this equation A_μ^a is the gluon field, that carries a Lorentz index and a group generator index, g_0 is the coupling constant of the strong interaction and the f^{abc} are the structure constants of $SU(3)$, which satisfy:

$$[t^a, t^b] = i f^{abc} t^c \quad (1.4)$$

with t^a being the generators of the algebra $\mathfrak{su}(3)$. The covariant derivative \mathcal{D} is defined then as:

$$\mathcal{D} = \gamma^\mu \partial_\mu - ig_0 \gamma^\mu t_a A_\mu^a \quad (1.5)$$

With the information contained in the lagrangian density the behavior and the interactions of all particles are set.

1.1.1 Feynman Rules of QCD

A key element that is needed to perform perturbative calculations in a quantum field theory are Feynman Rules. These are a set of equations and rules that represent the propagation of fields and the interaction vertices of the theory. For the case of QCD, being a non-abelian gauge theory, some vertices represent interactions between gauge bosons only, as opposed to Quantum Electrodynamics, QED, that forbids photon-photon interactions.

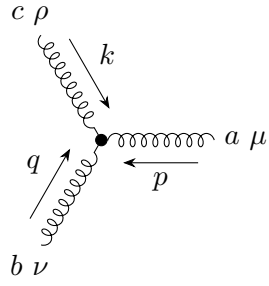
To begin with, we need to write out all of the terms of the lagrangian density individually. We assume only one quark flavor as no term in the lagrangian can change this quantum number.

$$\begin{aligned} \mathcal{L}_{QCD} &= -\frac{1}{4}(G_{\mu\nu}^a)^2 + \bar{\psi}(i\mathcal{D} - m)\psi \\ &= -\frac{1}{4} \left(\partial_\mu A_\nu^a - \partial_\nu A_\mu^a + g_0 f^{abc} A_\mu^b A_\nu^c \right) \left(\partial_\mu A_\nu^a - \partial_\nu A_\mu^a + g_0 f^{ade} A_\mu^d A_\nu^e \right) \\ &\quad + \bar{\psi}(i\gamma^\mu \partial_\mu + g_0 \gamma^\mu t_a A_\mu^a - m)\psi \\ &= -\frac{1}{4} (\partial_\mu A_\nu^a - \partial_\nu A_\mu^a)^2 \\ &\quad + \frac{1}{2} f^{abc} (\partial_\nu A_\mu^a - \partial_\mu A_\nu^a) [A^{b\mu}, A^{c\nu}] \\ &\quad - \frac{1}{4} g_0^2 f^{abc} f^{ade} A_\mu^b A_\nu^c A^{d\mu} A^{e\nu} \\ &\quad + g_0 \gamma^\mu t_a A_\mu^a \bar{\psi} \psi \\ &\quad + \bar{\psi}(i\gamma^\mu \partial_\mu - m)\psi \end{aligned} \quad (1.6)$$

First we define the gluon and quark propagators, which can be obtained from the first and last terms respectively:

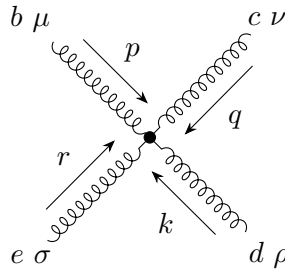
$$\begin{aligned} a \mu \xrightarrow{k} b \nu &= -\frac{i\delta_{ab}}{k^2 + i\epsilon} g^{\mu\nu} \\ i \xrightarrow{k} j &= \frac{i\delta_{ij}}{\not{k} - m + i\epsilon} \end{aligned} \quad \text{with}$$

$g^{\mu\nu}$ being the metric tensor of Minkovski space-time. The third term in eq. (1.6) represents a three gluon vertex:



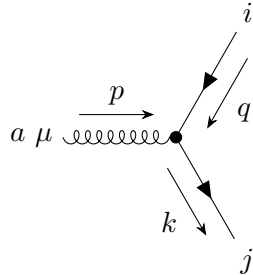
$$= -g f^{abc} [g^{\mu\nu}(p - q)^\rho + g^{\nu\rho}(q - k)^\mu + g^{\rho\mu}(k - p)^\nu]$$

Then the four-gluon vertex:



$$= -ig^2 [f^{abe} f^{acd} (g^{\mu\nu} g^{\sigma\rho} - g^{\mu\rho} g^{\nu\sigma}) \\ + f^{abd} f^{ace} (g^{\mu\nu} g^{\sigma\rho} - g^{\mu\sigma} g^{\nu\rho}) \\ + f^{abc} f^{aed} (g^{\mu\sigma} g^{\nu\rho} - g^{\mu\rho} g^{\nu\sigma})]$$

Finally we have the gluon-quark interaction vertex:



$$= -igt^a \gamma^\mu$$

Note that the lagrangian we considered, and the resulting Feynman rules, is over-simplified: the “full” lagrangian contains terms from Faddeev-Popov ghosts and counter-terms from the renormalization procedure. Nevertheless, interesting qualitative features can be inferred from the Feynman rules: the fact that gluons interact with each other through the three- and four-gluon vertices; the non flavor-changing interaction between gluons and quarks, which decouples completely different quark flavors; the “color-changing nature” of the quark-gluon interaction, given by the t^a matrix in the vertex term that shows how the color state of a fermion is changed by the absorption or emission of a gluon.

1.1.2 Gauge Symmetry of the Lagrangian

The QCD lagrangian must be gauge invariant to be physical. The concept of gauge invariance is crucial in the construction of a discretized lattice theory from the continuum one. Let’s consider

a quark field $\psi(x)$ and a local gauge transformation in the internal space of $SU(3)$ applied to it:

$$\psi(x) \rightarrow \psi'(x) = \Omega(x)\psi(x) \quad : \quad \Omega(x) = \exp(i(\alpha^a(x)t^a)) \quad (1.7)$$

here $\Omega(x)$ is an element of the $SU(3)$ gauge group. This transformation if applied to the simple Dirac free-field Lagrangian would generate an additional term:

$$\begin{aligned} \mathcal{L}_{Dirac} = \bar{\psi}(i\gamma^\mu \partial_\mu - m)\psi &\rightarrow \mathcal{L}'_{Dirac} = \bar{\psi}\Omega^\dagger(i\gamma^\mu \partial_\mu - m)(\Omega\psi) \\ &= \bar{\psi}'(i\gamma^\mu \partial_\mu - m)\psi' + i\bar{\psi}'\gamma^\mu \psi(\partial_\mu \Omega) \end{aligned} \quad (1.8)$$

In order to fix this problem a new field $A_\mu(x)$, the gauge field, is introduced and it enters the definition of the covariant derivative, so that ∂_μ becomes $D_\mu = \partial_\mu - ig_0 A_\mu(x)$ as previously stated. The transformation rule for $A_\mu(x)$ is fixed in order to cancel the extra term in eq. (1.8) exactly, such that:

$$D_\mu \psi \rightarrow (D_\mu \psi)' = (\partial_\mu - ig_0 A'_\mu(x))\psi' = \Omega(D_\mu \psi) \quad (1.9)$$

and this fixes the transformation for $A_\mu(x)$ to be:

$$A_\mu(x) \rightarrow A'_\mu(x) = \Omega \left[A_\mu(x) - \frac{i}{g_0} \Omega^\dagger \partial_\mu \Omega \right] \Omega^\dagger \quad (1.10)$$

we can see that the last term contributes effectively to the lagrangian as $-i\bar{\psi}'\gamma^\mu \psi(\partial_\mu \Omega)$, which is what we want to cancel. For an infinitesimal transformation we can expand the matrix Ω and get the following for the gauge field transformation:

$$A_\mu^a(x) \rightarrow A'^a_\mu(x) = \alpha^a(x) - \frac{i}{g_0} \partial_\mu \alpha^a(x) + f^{abc} \alpha^b(x) \alpha^c(x) \quad (1.11)$$

which is the last element needed. One can now look at all the possible gauge invariant objects that can be constructed with the fields ψ and A of order 4, the same of the lagrangian. Apart from the one already present in the Dirac lagrangian with the covariant derivative, there are only two additional terms that are gauge invariants and of order 4 and they both can be taken by considering the gauge field tensor:

$$G_{\mu\nu}^a \equiv \frac{i}{g_0} [D_\mu, D_\nu] = \partial_\mu A_\nu^a - \partial_\nu A_\mu^a + g_0 f^{abc} A_\mu^b A_\nu^c \quad (1.12)$$

this is clearly gauge invariant since it is commutator of covariant derivatives and it has dimension 2. One can now construct the gauge field kinetic term, the well known $-\frac{1}{4}(G_{\mu\nu}^a)^2$ and reconstruct eq. (1.2). However, there is an additional term, not included in the QCD lagrangian, that is the “dual term”, or “theta term” which will be interesting further in the work. It is defined as $\theta G_{\mu\nu}^a \tilde{G}^{a\mu\nu}$ where $\tilde{G}^{a\mu\nu} = \epsilon^{\mu\nu\rho\sigma} G_{\rho\sigma}^a$ is the dual of the field tensor and $\epsilon_{\mu\nu\rho\sigma}$ the anti-symmetric Levi-Civita tensor. With it the lagrangian becomes:

$$\mathcal{L}_{QCD} = -\frac{1}{4}(G_{\mu\nu}^a)^2 + \bar{\psi}(i\not{D} - m)\psi + \theta G_{\mu\nu}^a \tilde{G}^{a\mu\nu} \quad (1.13)$$

The theta term is usually neglected because there is no experimental evidence of it, but in principle it cannot be excluded. It is the simplest CP violating term that can be added to the QCD lagrangian and for this is of particular interest in the study of \mathcal{CP} phenomena, like the nucleon electric dipole moment (EDM)[3].

1.2 General Properties of QCD

Quantum Chromodynamics exhibits a set of features as a theory that are common to all non-abelian gauge theories. We have already seen one, that is the direct interaction of the gauge bosons, something that is not allowed in abelian theories as QED. Other interesting properties emerge when trying to renormalize the theory and are in general linked to the fixing of the scale, which leads to the concept of running coupling. In the particular case of QCD the coupling constant at in a low-energy regime leads to Confinement, while in the high-energy limit Asymptotic Freedom emerges.

1.2.1 Running Coupling

The Renormalization Group Equation (RGE) defines the rate at which the renormalized coupling varies as the renormalization scale of μ changes, through the beta function of the coupling constant, $\beta(g_0)$.

$$\beta(g_0) = \frac{d}{d \log(\mu)} g_0(\mu) \quad (1.14)$$

For a generic non-abelian theory $SU(N)$ one can expand the β function in orders of g as:

$$\beta(g_0) = b_0 g_0^3 + b_1 g_0^5 + b_2 g_0^7 + \dots \quad (1.15)$$

One can then integrate up to arbitrary order eq. (1.14) and get an expression for $g_0(\mu)$. The coefficients b_i are obtained from computing contribution of higher and higher diagrams to the coupling. The value of b_0 , from 1-loop corrections, is:

$$b_0 = -\frac{g_0^3}{(4\pi)^2} \left(\frac{11}{3}N - \frac{2}{3}N_f \right) \quad (1.16)$$

the minus sign in front implies that any non-abelian theory with a sufficiently small number of fermions, less than $\frac{11}{2}N$ (that is 16 for QCD), is “asymptotically free”, meaning that at high energy the coupling vanishes and particles don’t feel any interaction.

The RGE is usually expressed in terms of the analog of the fine structure-constant for the strong force, $\alpha_s = g_0^2/4\pi$. The first order solution is given by plugging eq. (1.16) into eq. (1.14) and integrating. In terms of α_s at a scale μ we get:

$$\alpha_s(\mu) = \frac{\alpha_s}{1 + \frac{b_0 \alpha_s}{4\pi} \log(\mu^2/M^2)} \quad (1.17)$$

The typical choice for μ when measuring experimentally the running coupling is the mass of the Z boson, where QCD can be compared relatively simply to the other forces and experimental precision is high. The coupling depends on an arbitrarily chosen renormalization point M . A convenient choice is to define a momentum scale Λ that satisfies:

$$1 = \alpha_s^2 \left(\frac{b_0}{4\pi} \right) \log(M^2/\Lambda^2) \quad (1.18)$$

This simplifies eq. (1.17) to its well-known form, correct up to one loop corrections:

$$\alpha_s(\mu) = \frac{4\pi}{b_0 \log(\mu^2/\Lambda^2)} \quad (1.19)$$

In fig. 1.2 a higher order approximation of $\alpha_s(\mu)$ is plotted against some experimental values. In section 3.4.1 we will show a more precise result, correct up to order 4, of this result. The

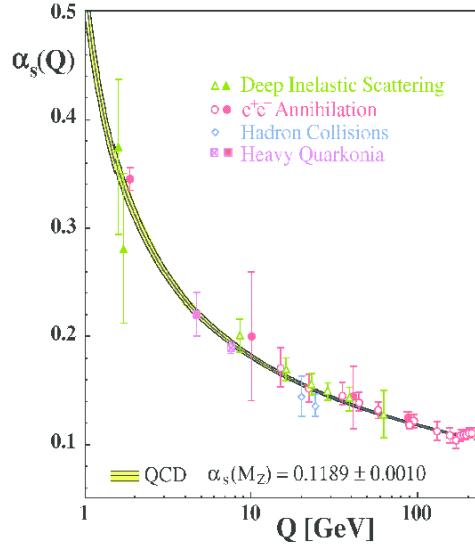


Figure 1.2: The strong coupling as a function of the energy scale. Image from [4]

momentum scale, often referred to as Λ_{QCD} , is the energy at which the interactions become strong. Experimental values [5] suggest that $\Lambda \approx 200 - 300$ MeV, meaning that perturbation theory can be safely applied from momenta roughly above the 1 GeV scale, where $\alpha_s \approx 0.4$. Our main goal for this thesis is to find a simple and not expensive way to estimate the mass scale parameter Λ from lattice calculations, in this work on pure Yang-Mills theory, that means with no fermion flavors, and in prospect for QCD with 2 or 2 + 1 dynamical fermions.

Asymptotic Freedom

Equation (1.19) is a clear indication that QCD at high energies has a small coupling. Asymptotic freedom is the property of gauge theories, QCD is usually the example for it, that causes the interactions between the fields do become weaker as the energy scale increases. This is for example one of the basis on which unification theories are based on, the fact that there exists an energy scale at which the strong force has a coupling equivalent to the one of the electroweak interaction. The discovery of asymptotic freedom by Gross, Wilczek and Politzer [6][7], was used as an indication that QCD is indeed the correct theory of the strong interaction in the late Seventies, when the fundamental theory was still debated.

Asymptotically free theories, can be analyzed perturbatively at sufficiently large energies and are believed to be consistent up to any energy scale.

Confinement

At low energy scales from eq. (1.19) we can infer that the coupling constant increases exponentially and approaches 1. This is the reason for the fundamentally different nature of the strong force compared to the other forces, no perturbative expansion can be made at low energies. The exact proof of how this links with the color confinement of QCD is yet not known, but qualitatively it can be explained by the fact that the gauge bosons of the theory, the gluons, carry color charge just like the quarks.

Lambda One can also look at the inverse of the momentum scale and find that the interactions between color charges become strong at a distance $1/\Lambda \approx 1 \text{ fm}$, which is of the order of the radius of the light hadrons. In general color charged particles cannot be isolated, so that quarks and gluons are not detectable alone, but always in the form of hadrons: colorless objects formed of multiple quarks, mesons (quark-anti-quark) and hadrons (three quarks or three anti-quarks). Also glueballs, combinations of gluons such that the total is colorless, are in principle allowed, but have not been observed yet. Confinement is the phenomenon for which it is not possible to isolate a color charge, single quarks or gluons, from a hadron without producing other new hadrons. Single colored particle in a very small time scale undergo hadronization, the process of spawning new quarks or anti-quarks from the vacuum to balance the total color charge and produce colorless matter.

The other usual picture is to consider the gluons being exchanged by two quarks to form flux-tubes that, if stretched by separating the quark sources, eventually store enough energy to make a quark-anti-quark pair energetically favorable, as depicted in fig. 1.3

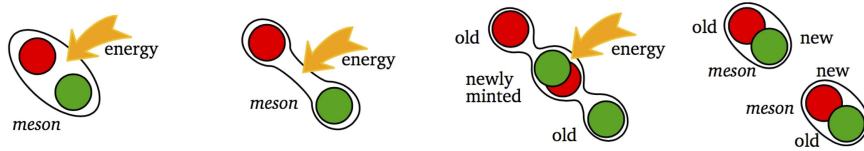


Figure 1.3: Representation of confinement using flux-tubes. As two color sources are pulled apart, the energy stored in the color field between the sources increases so much that a $q\bar{q}$ pair is formed from the vacuum energy.

1.3 Methods and Regimes of Chromodynamics

Given the very different behaviors of the strong force at different energy scales, QCD needs to be dealt with in various ways depending on the scale of interest. At high energies perturbation theory can be applied safely, but at low energies no expansion in the coupling constant can be made.

Perturbative QCD

At high energies, like the scale of the large particle accelerators that are colliders currently available, the QCD coupling constant is sufficiently small to allow analytical calculations of Feynman diagrams to be meaningful. Hadronization is neglected as the time scale is small enough to consider it a post-collision process. For example, at a scale where the strong force is comparable to the electroweak interaction, the cross section of $e^+e^- \rightarrow \text{hadrons}$ compared to that of $e^+e^- \rightarrow \mu^+\mu^-$ can be used to measure the number of quark flavors that are active below that energy. Figure (1.4) the perturbative QCD cross section for the process is shown compared to experimental data.

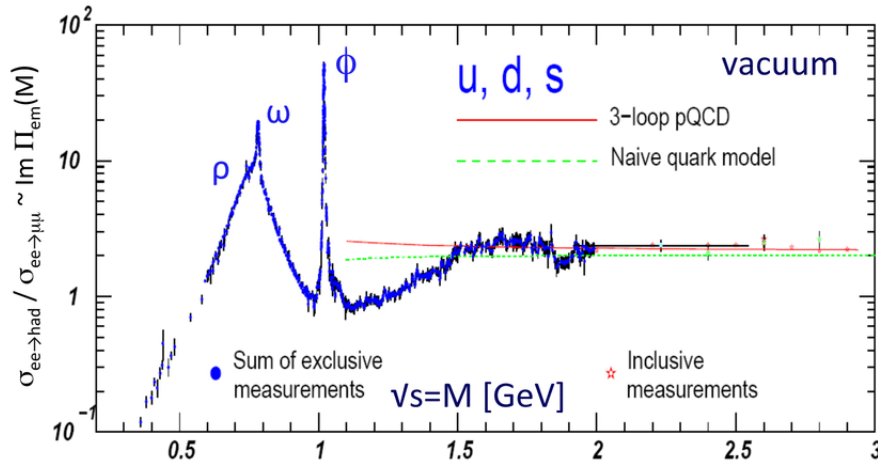


Figure 1.4: Ratio of the experimental cross section of $e^+e^- \rightarrow \text{hadrons}$ and $e^+e^- \rightarrow \mu^+\mu^-$; pQCD results are also shown to agree well to experiment in non resonant regions of the energy spectrum. [8]

Lattice Methods

To deal with the non-perturbative sector of the strong interaction the most widespread approach is to use numerical simulations, in particular lattice methods, so it is common to refer to it as Lattice QCD. The main idea, which will be expressed more in detail in Chapter 2, is to discretize space-time and evaluate the field only at fixed sites on a hyper-cubic lattice, physical quantities are then computed stochastically on ensembles of such gauge fields. This approach however is very expensive from a computational point of view and so far no calculation at physical quark masses with a sufficiently small lattice spacing, in principle closer to the continuum theory, have been performed.

Effective Field Theories

An interesting problem is to link QCD directly with nuclear forces, that are long range remnants of the strong interaction at a hadron level. The problem is of high interest because there is yet no fundamental theory of nuclear interactions from first principles. The most common approach is to define an Effective Field Theory, starting from a low energy approximation of chromodynamics, that preserves most of the symmetries of the underlying theory.

Chiral EFT (χEFT) is one of the most popular approaches, it starts from considering nucleons as a fundamental $SU(2)$ group in isospin and describes the interactions between them through the exchange of pions [9]. It promotes particles that are not fundamental in QCD to the basic blocks of a low-energy effective lagrangian, with nucleons as the fermion fields and pions as Nambu-Goldstone bosons of the theory. Its lagrangian is constructed in a systematic manner considering all possible interaction vertices between hadrons:

$$\mathcal{L}_{\chi EFT} = \mathcal{L}_{\pi\pi} + \mathcal{L}_{\pi N} + \mathcal{L}_{NN} + (\text{three hadron terms}) + \dots \quad (1.20)$$

where $\mathcal{L}_{\pi\pi}$ is the term describing the dynamics between pion, \mathcal{L}_{NN} the term for interactions between two nucleons, $\mathcal{L}_{\pi N}$ the one between one pion and one nucleon and so on. Each term is further expanded in powers of Q/Λ_χ where Q is the pion momentum and Λ_χ is the energy scale at which the theory breaks down because of the pions acquiring an energy comparable to the mass of the nucleons. One constructs order by order all possible terms:

$$\begin{aligned} \mathcal{L}_{NN} &= \mathcal{L}_{NN}^{(0)} + \mathcal{L}_{NN}^{(2)} + \mathcal{L}_{NN}^{(4)} + \dots \\ \mathcal{L}_{\pi N} &= \mathcal{L}_{\pi N}^{(1)} + \mathcal{L}_{\pi N}^{(2)} + \mathcal{L}_{\pi N}^{(3)} + \mathcal{L}_{\pi N}^{(4)} + \dots \\ \mathcal{L}_{\pi\pi} &= \mathcal{L}_{\pi\pi}^{(2)} + \mathcal{L}_{\pi\pi}^{(4)} + \dots \end{aligned} \quad (1.21)$$

one then computes all possible diagrams order by order and truncates the expansion when needed. This is mostly useful for computing reduced matrix elements for many-body nuclear calculations.

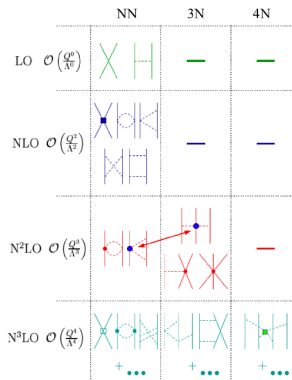


Figure 1.5: Diagrams of the leading order terms in χEFT . [10]

One interesting remark, as seen in fig. 1.5 is that the approach of χEFT spontaneously generates interaction matrix elements for three or more nucleons.

Chapter 2

Lattice Field Theories and Lattice QCD

Lattice QCD is one of the main Lattice Field Theories. It deals with the strong force in a numerical way. The idea of discretizing space-time in a lattice and perform calculations of field theories was proposed by Wilson in 1974 [11] as an alternative method to explain confinement. It has proven to be the most systematic approach to non-perturbative theories like QCD. In this chapter we will describe briefly how this discretization procedure is performed and some of the main computational strategies that are involved.

2.1 Discretizing Field Theories

The starting point for Lattice QCD is Feynman's path-integral formalism, but expressed in Euclidean space-time, through a Wick rotation. An observable of some field ϕ is then given by:

$$\langle O[\phi] \rangle = \frac{1}{Z[\phi]} \int \mathcal{D}[\phi] O[\phi] e^{-S[\phi]} \quad (2.1)$$

where the partition function $Z[\phi]$ is defined as:

$$Z = \int \mathcal{D}[\phi] e^{-S[\phi]} \quad (2.2)$$

and $S[\phi]$ is the classical action of the field. Evaluating path-integrals is not possible in general with analytical tools so, in order to allow numerical computations, the Euclidean space-time is discretized on a hyper-cubic lattice $L = (L_x, L_y, L_z, L_t)$. The choice of the lattice spacing, usually denoted a , is arbitrary, but most often it is chosen to be equal for all dimensions. if we then define a lattice site $n = (n_x, n_y, n_z, n_t)$ where all the n s represent the coordinates of a point in the lattice Λ , our fields are constrained to have values on the points an instead of on a continuum space-time x^μ .

$$\phi(x) \xrightarrow{\text{discretization}} \phi(an) \quad (2.3)$$

2.1.1 The Harmonic Oscillaor Example

2.2 Discretization of QCD on the Lattice

In the case of QCD there are two types of field at play, the gluon gauge field A and the n_f fermionic quark fields ψ .

2.2.1 Naïve Discretization of Fermions

In this section the fermion discretization procedure found in [12] is followed, but also some elements from [13], quoting the main intermediate steps that lead to the formulation of Lattice QCD. The starting point is the fermionic euclidean action in the continuum:

$$S_F[\psi, \bar{\psi}] = \int dx^4 \bar{\psi}(x) (\gamma_\mu \partial^\mu + m) \psi(x) \quad (2.4)$$

now we discretize the euclidean space-time on a lattice Λ of spacing a , each point will be denoted with n . The partial derivative can be turned into the central finite difference between neighboring points along the direction of the derivative:

$$\partial_\mu \psi(x) \rightarrow \frac{\psi(n + \hat{\mu}) - \psi(n - \hat{\mu})}{2a} \quad (2.5)$$

The discretized fermion action is then:

$$S_F[\psi, \bar{\psi}] = a^4 \sum_{n \in \Lambda} \bar{\psi}(n) \left[\sum_{\mu=1}^4 \gamma_\mu \frac{\psi(n + \hat{\mu}) - \psi(n - \hat{\mu})}{2a} + m \psi(n) \right] \quad (2.6)$$

As we did in section 1.1.2 we try to apply a local gauge transformation $\Omega(n)$ to the field. It is simple to show that the terms of the derivative in the action are not gauge invariant:

$$\bar{\psi}(n) \psi(n \pm \hat{\mu}) \rightarrow \bar{\psi}(n) \Omega^\dagger(n) \Omega(n \pm \hat{\mu}) \psi(n \pm \hat{\mu}) \quad (2.7)$$

The problem is in the way the derivative was discretized, it also removed one Lorentz index so it had to be wrong, and the solution is the introduction of an additional field as in 1.1.2 that has the correct transformation laws. This field must connect the values of the fermion field at two different lattice sites and because of this it is denoted "link variables" and by convention it is denoted as $U(n, n + \hat{\mu}) = U_\mu(n)$. Furthermore, it must depend on the orientation along the μ direction in a simple way:

$$U(n, n - \hat{\mu}) \equiv U_{-\mu}(n) = U_\mu(n - \hat{\mu})^\dagger \quad (2.8)$$

In particular, we want it to transform as:

$$\begin{aligned} \bar{\psi}(n) U_\mu(n) \psi(n + \hat{\mu}) &\rightarrow \bar{\psi}(n) \Omega^\dagger(n) U'_\mu(n) \Omega(n + \hat{\mu}) \psi(n + \hat{\mu}) \\ \bar{\psi}(n) U_{-\mu}(n) \psi(n - \hat{\mu}) &\rightarrow \bar{\psi}(n) \Omega^\dagger(n) U'_{-\mu}(n) \Omega(n - \hat{\mu}) \psi(n - \hat{\mu}) \end{aligned} \quad (2.9)$$

from which we infer that:

$$\begin{aligned} U_\mu(n) &\rightarrow U'_\mu(n) = \Omega(n)U_\mu(n)\Omega^\dagger(n + \hat{\mu}) \\ U_{-\mu}(n) &\rightarrow U'_{-\mu}(n) = \Omega(n)U_{-\mu}(n)\Omega^\dagger(n - \hat{\mu}) \end{aligned} \quad (2.10)$$

the field $U_\mu(n)$ which we identify with the link variables depends on the direction of the move along the μ direction. A visual representation is given in fig. 2.1,



Figure 2.1: Schematic representation of the link variables $U_\mu(n)$ and $U_{-\mu}(n)$ on the lattice.

With this results we can write a gauge invariant lattice fermion action as:

$$S_F[\psi, \bar{\psi}] = a^4 \sum_{n \in \Lambda} \bar{\psi}(n) \left[\sum_{\mu=1}^4 \gamma_\mu \frac{U_\mu(n)\psi(n + \hat{\mu}) - U_{-\mu}(n)\psi(n - \hat{\mu})}{2a} + m\psi(n) \right] \quad (2.11)$$

2.2.2 The Gauge Transporter and the Wilson Loop

A more formal definition of the link variables we can look at the gauge transporter. This is the path-ordered product, denoted with \mathcal{P} of a gauge field $A(x)$ along some curve \mathcal{C} between two points in space-time:

$$G(x, y) = \mathcal{P} \exp \left(i \int_x^y A(x') dx' \right) \quad (2.12)$$

An important thing to note now is that link variables belong to the gauge group, $SU(3)$ for QCD, and not to the algebra, $\mathfrak{su}(3)$. With this definition is easy to see the relation we just stated earlier on the direction change:

$$U(n, n - \hat{\mu}) = U_{-\mu}(n) = U_\mu^\dagger(n) \quad (2.13)$$

In the continuum case it can be shown, in [2] for example, that the trace of a gauge transporter that has the same start and final point, a Wilson Loop, is gauge invariant. On the lattice the minimal Wilson loop is just a square:

$$\begin{aligned} P_{\mu\nu}(n) &= U_\mu(n)U_\nu(n + \hat{\mu})U_{-\mu}(n + \hat{\mu} + \hat{\nu})U_{-\nu}(n + \hat{\nu}) \\ &= U_\mu(n)U_\nu(n + \hat{\mu})U_\mu^\dagger(n + \hat{\nu})U_\nu^\dagger(n) \end{aligned} \quad (2.14)$$

a pictorial representation is given in fig. 2.2.

Up to order $\mathcal{O}(a)$ the integral on the straight line connecting two points on the lattice can be approximated with $aA_\mu(n)$, giving us $U_\mu(n) = \exp(iaA_\mu(n))$. This allows us to write using the

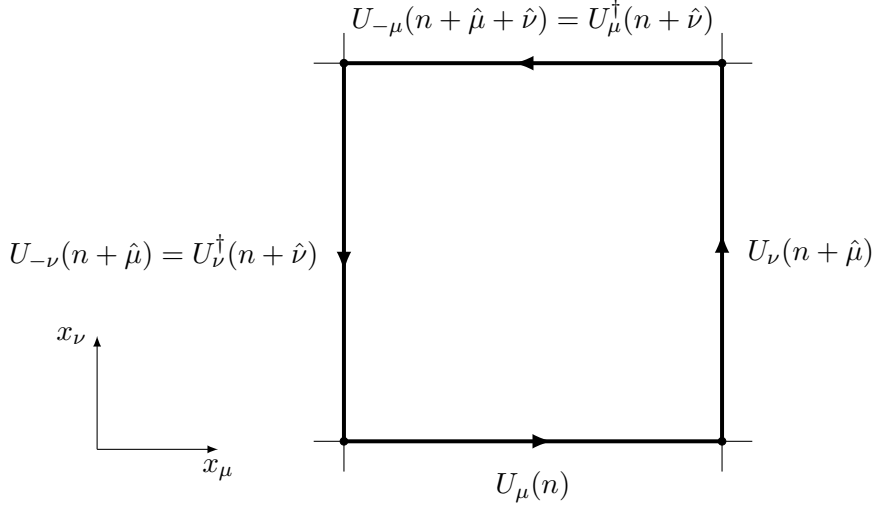


Figure 2.2: The Plaquette, as defined on the lattice, it terms of the oriented product of the link variables of a minimal square in the plane $\mu\nu$.

Baker-Campbell-Hausdorff formula:

$$\begin{aligned}
 P_{\mu\nu}(n) = \exp & \left[iaA_\mu(n) + iaA_\nu(n + \hat{\mu}) - iaA_\mu(n + \hat{\nu}) - iaA_\nu^\dagger(n) - \frac{a^2}{2}[A_\mu(n), A_\mu(n + \hat{\mu})] \right. \\
 & - \frac{a^2}{2}[A_\nu(n + \hat{\nu}), A_\nu(n)] + \frac{a^2}{2}[A_\mu(n), A_\nu(n)] + \frac{a^2}{2}[A_\nu(n + \hat{\mu}), A_\mu(n + \hat{\nu})] \\
 & \left. + \frac{a^2}{2}[A_\mu(n), A_\mu(n + \hat{\nu})] + \frac{a^2}{2}[A_\nu(n + \hat{\mu}), A_\nu(n)] + \mathcal{O}(a^3) \right]
 \end{aligned} \tag{2.15}$$

Now the terms that are shifted from the site n are expanded as:

$$A_\mu(n + \hat{\nu}) = A_\mu(n) + a\partial_\nu A_\mu(n) + \mathcal{O}(a^2) \tag{2.16}$$

and with this substitution most terms cancel and we are left with:

$$\begin{aligned}
 P_{\mu\nu}(n) &= \exp [ia^2(\partial_\mu A_\nu(n) - \partial_\nu A_\mu(n) + i[A_\mu(n), A_\nu(n)]) + \mathcal{O}(a^3)] \\
 &= \exp [ia^2 F_{\mu\nu}(n) + \mathcal{O}(a^3)]
 \end{aligned} \tag{2.17}$$

This term can be used to build the euclidean lattice action term for the gluons. In particular, we would like a term of the form:

$$S_G[U] = \frac{a^4}{2g^2} \sum_{n \in \Lambda} \sum_{\mu\nu} \text{Tr}(F_{\mu,\nu}(n)^2) \tag{2.18}$$

Up to order $\mathcal{O}(a^2)$ this can be obtained by:

$$S_G[U] = \frac{2}{g^2} \sum_{n \in \Lambda} \sum_{\mu < \nu} \Re \text{Tr}(\mathbf{1} - P_{\mu\nu}(n)) \tag{2.19}$$

Higher order corrections to this action can be computed analytically by considering higher orders in the BCH expansion and in the exponential expansion when constructing 2.19.

2.2.3 Lattice Fermions

The discretization of fermions as discussed in the previous section is incomplete. It becomes evident if one considers the Fourier transform of the propagator. Let's first rewrite 2.11 in a more compact way, introducing the lattice Dirac propagator $M_{xy}[U]$.

$$S_F[\psi, \bar{\psi}] = \sum_{n \in \Lambda} \bar{\psi}(x) M_{xy}[U] \psi(y) \quad (2.20)$$

with

$$M_{xy}[U] = \sum_{\mu=1}^4 \gamma_{\mu} \frac{U_{\mu}(x) \delta_{x, (y-\hat{\mu})} - U_{-\mu}^{\dagger}(x) \delta_{x, (y+\hat{\mu})}}{2a} + m \delta_{x,y} \quad (2.21)$$

in momentum space the propagator becomes:

$$\tilde{M}_{pq} = \delta(p-q) \tilde{M}(p) \quad : \quad \tilde{M}(p) = m \mathbb{1} + \frac{i}{a} \sum_{\mu=1}^4 \gamma_{\mu} \sin(p_{\mu} a) \quad (2.22)$$

In order to calculate the inverse of the propagator in real space we need to invert the one in momentum space and perform an inverse Fourier transform. However, the inverse of the propagator in Fourier space has multiple poles:

$$\tilde{M}(p)^{-1} \Big|_{m=0} = \frac{-ia \sum_{\mu} \gamma_{\mu} \sin(p_{\mu} a)}{\sum_{\mu} \sin^2(p_{\mu} a)} \quad (2.23)$$

the problem vanishes for $a \rightarrow 0$, the continuum case, returning just one fermion type, but on the lattice multiple fermions. This is known as the “doubling problem”. The solution, proposed by Wilson, is to modify the propagator adding some terms that make the poles in the inverse of the Fourier transformed propagator vanish. The final form of the Wilson Fermion Action is:

$$S_F[\psi, \bar{\psi}] = \sum_{n \in \Lambda} \bar{\psi}(x) M_{xy}^W[U] \psi(y) \quad (2.24)$$

with $m_{xy}^W[U]$ being the Wilson propagator:

$$M_{xy}^W[U] = \frac{1}{2a} \sum_{\mu=\pm 1}^{\pm 4} (\mathbb{1} - \gamma_{\mu}) U_{\mu}(x) \delta_{x, (y-\hat{\mu})} + \left(m + \frac{4}{a}\right) \delta_{x,y} \quad (2.25)$$

the shorthand notation $\gamma_{-\mu} = -\gamma_{\mu}$ has been introduced.

Now that all the needed information about the action and the fields is set, mainly through equations 2.11 and 2.24, the picture of how to discretize QCD from the continuum Minkowski space-time to an euclidean space-time lattice.

2.3 Path Integrals on the Lattice

To express expectation values and correlators on the lattice, path integral formalism is used. The partition function, as we have seen earlier, is the path integral of the fields over the whole

space of the action. For the case of QCD the fields are U , ψ and $\bar{\psi}$:

$$Z = \int \mathcal{D}\psi \mathcal{D}\bar{\psi} \mathcal{D}U e^{-S[\psi, \bar{\psi}, U]} \quad (2.26)$$

with the action being the sum of the gluonic and fermionic parts:

$$S[\psi, \bar{\psi}, U] = S_G[U] + S_F[\psi, \bar{\psi}, U] = S_G[U] + \sum_f \bar{\psi} M \psi \quad (2.27)$$

The immediate simplification is to integrate out the fermion fields. As in the continuum case one can perform an integration on the Grassmann-valued fields, in general for an integral over some Grassmann numbers θ_i and their complex conjugates θ_i^* , and a Hermitean matrix K :

$$\begin{aligned} \int \mathcal{D}\theta^* \mathcal{D}\theta e^{-\Theta K \Theta} &= \left(\prod_i \int d\theta_i^* d\theta_i \right) e^{-\theta_i^* K_{ij} \theta_j} = \left(\prod_i \int d\theta_i^* d\theta_i \right) e^{-\sum_i \theta_i^* k_i \theta_i} \\ &= \prod_i b_i = \det B \end{aligned} \quad (2.28)$$

This result is very different from what one would get in the real case, $(2\pi)^n / \det B$. It can also be shown that:

$$\begin{aligned} \int \mathcal{D}\theta^* \mathcal{D}\theta \theta_a^* \theta_b e^{-\Theta K \Theta} &= \left(\prod_i \int d\theta_i^* d\theta_i \right) \theta_a^* \theta_b e^{-\theta_i^* K_{ij} \theta_j} = \left(\prod_i \int d\theta_i^* d\theta_i \right) \theta_a^* \theta_b e^{-\sum_i \theta_i^* k_i \theta_i} \\ &= (\det B) (B^{-1})_{ab} \end{aligned} \quad (2.29)$$

This last result is crucial for computing fermion propagators for example, for a given “source” $\bar{\psi}(x)$ and a “sink” $\psi(y)$ the propagator between the two can be computed via path integrals, but it requires inverting the fermion action matrix.

With the result of 2.28 we can simplify greatly the partition function:

$$Z = \int \mathcal{D}\psi \mathcal{D}\bar{\psi} \mathcal{D}U e^{-S[\psi, \bar{\psi}, U]} = \int \mathcal{D}U e^{-S_G[U]} \det M[U] \quad (2.30)$$

In a similar fashion as in statistical mechanics, the expectation value of an observable on the lattice can be computed as:

$$\langle O \rangle = \frac{1}{Z} \int \mathcal{D}U O(\psi, \bar{\psi}, U) e^{-S_G[U]} \det M[U] \quad (2.31)$$

The above expression cannot be evaluated or simplified analytically any further, so the usual approach is to approximate the path integral numerically. The main idea is to create an ensemble of field configurations to reproduce the integral $\int \mathcal{D}$, on such set $\mathcal{U} = \{U_1, U_2, \dots, U_N\}$ one computes the observable and the average value is the expectation value of the observable:

$$\langle O \rangle \approx \frac{1}{N} \sum_{i=1}^N O(\psi, \bar{\psi}, U_i) \quad (2.32)$$

The choice of the set \mathcal{U} is the interesting part, and it starts from identifying parts of 2.31 as a probability distribution, in particular, the probability of a configuration U is identified with:

$$P[U] = \frac{e^{-S_G[U]} \det M}{Z} \quad (2.33)$$

The integral is then evaluated using Monte Carlo integration, where the different configurations are chosen in the most widely accepted solution via a Markov chains. Given a field configuration U_i one chooses the following configuration U_{i+1} only based on properties of U_i . Later we will see how the Metropolis algorithm, one of the simplest Markov Chain Monte Carlo methods has been implemented.

2.3.1 Pure Gauge Field Theory

Computing full QCD on the lattice is computationally expensive, mainly due to the integration of fermions via the determinant. From a numerical point of view, the determinant need to be computed at every step of the Markov chain that is used to evaluate the path-integral and this operation affects the time cost of sampling the configuration space dramatically. A first approach is to neglect the determinant completely, considering it constant. This is effectively removing dynamical fermions, freezing them to the lattice sites. This approximation is usually referred to as “quenched QCD”, or QQCD. The properties of this theory, that is then reduced to a simple Yang-Mills theory are still interesting to study and have played historically a very important role, being the only accessible simulation until sufficient computing power became available.

2.3.2 Observables

On the lattice, given the transformation 2.10, any product of link variables that starts and end at the same lattice-site, a closed loop, is gauge invariant. The average values of these objects over the whole lattice can be linked to physical observables, for example the field tensor. In a more general form any observable $L[U]$ defined as

$$L[U] = \text{Tr} \left[\prod_{(n,\mu) \in \mathcal{L}} U_\mu(n) \right] \quad (2.34)$$

where \mathcal{L} is a closed loop of links on the lattice is a gauge invariant object and a candidate observable.

Plaquette

The simplest observable, which we have already encountered upon defining the Wilson action in 2.11, is the plaquette. This is the minimal closed loop on the lattice and its value is related to the coupling constant of the action. For each lattice site there are 12 possible plaquettes

to be computed, given all the combinations of euclidean indices. A proper definition of the observable is:

$$P[U] = \frac{1}{6|\Lambda|} \sum_{n \in \Lambda} \sum_{\mu < \nu} P_{\mu\nu}(n) \quad (2.35)$$

where $P_{\mu\nu}(n)$ is the one defined in eq. (2.15). As a side note, in actual calculations at every lattice site only the positive sign link variables are stored, so the second line of 2.15 is the one that is actually used in simulations.

Energy Density

The energy of the field is proportional to the square of the field tensor, in particular:

$$E[U] = -\frac{1}{4|\Lambda|} \Re \text{Tr}(G_{\mu\nu} G^{\mu\nu}) \quad (2.36)$$

In order to estimate this quantity, one has to compute the field tensor at every lattice site, square it and sum over the whole space. It is then usually normalized by the lattice volume (the number of sites), to get the density. The simplest definition of the field tensor is $G_{\mu\nu}^{(plaq)} = \mathbb{1} - P_{\mu\nu}$ but this is not very accurate. A more symmetric definition can be obtained by the “clover”, that is summing all the plaquettes of a same plane $\mu\nu$ that start from a given lattice site.

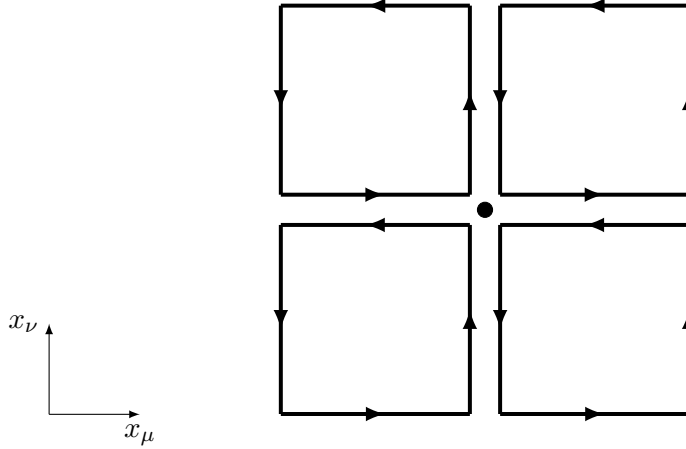


Figure 2.3: Schematic representation of the symmetric definition of the clover term $G_{\mu\nu}^{(clover)}$ on the lattice.

In terms of link variables this is equal to:

$$\begin{aligned} G_{\mu\nu}^{(clover)}(n) = \frac{1}{4} \Big[& U_\mu(n) U_\nu(n + \hat{\mu}) U_\mu^\dagger(n + \hat{\nu}) U_\nu^\dagger(n) \\ & - U_\nu(n) U_\mu^\dagger(n + \hat{\nu}) U_\nu^\dagger(n - \hat{\mu}) U_\mu(n - \hat{\mu}) \\ & + U_\mu^\dagger(n - \hat{\mu}) U_\nu^\dagger(n - \hat{\mu} - \hat{\nu}) U_\mu(n - \hat{\mu} - \hat{\nu}) U_\nu(n - \hat{\nu}) \\ & - U_\nu^\dagger(n - \hat{\nu}) U_\mu(n - \hat{\nu}) U_\nu(n + \hat{\mu} - \hat{\nu}) U_\mu^\dagger(n) \Big] \end{aligned} \quad (2.37)$$

Topological Charge

The gauge fields in QCD exhibit particular topological properties that are believed to have important physical implications [14][15]. The topological charge is an integer quantum number of the field in the continuum, but on the lattice certain definitions can be used to reproduce the continuum properties, especially for the so called “topological susceptibility”, that is the second moment of the distribution of the topological charge, which seems to be independent from the definitions of the base observable [16]. In the continuum topological sectors, regions of space with same charge, are separated from each other, on the lattice through discretization effects the behavior is different, with instantons that allow tunneling between sectors [17].

The topological charge is the integral over all space-time of the topological charge density:

$$Q = \int d^4x q(x) \quad (2.38)$$

where

$$q(x) = \frac{1}{64\pi^2} \text{Tr}(F_{\mu\nu} \tilde{F}^{\mu\nu}) \quad (2.39)$$

with $\tilde{F}^{\mu\nu} = \frac{1}{2} \epsilon^{\mu\nu\rho\sigma} F_{\rho\sigma}$. This can be estimated on the lattice, in the simplest way, by using the same definition of the field strength tensor we used before for the energy density, the clover:

$$Q[U] = \frac{1}{64\pi^2} \sum_{n \in \Lambda} \sum_{\mu < \nu} \epsilon^{\mu\nu\rho\sigma} \text{Tr}[G_{\mu\nu}^{(\text{clover})}(n) G_{\rho\sigma}^{(\text{clover})}(n)] \quad (2.40)$$

As the lattice spacing is reduced, approaching the continuum, the topological sectors get more and more separated, preventing tunneling between them. This makes the Markov chain used to generate the ensemble less efficient in terms of growing autocorrelation times, as will be shown in section 5.2.

A derived quantity of great interest is the topological susceptibility χ , that is proportional to the expectation value of the square of the topological charge:

$$\chi = \frac{\hbar c}{a^4 |\Lambda|} \langle Q^2 \rangle \quad (2.41)$$

This observable is particularly important for the properties of instantons on the lattice and its value can be related via the Witten-Veneziano formula to the mass of the η' .

2.4 Modern Lattice QCD Calculations

motlo vaga...

The state of the art calculations in Lattice QCD involve improved fermion and gluon actions. For the gluon sector the improvements are based on finding linear combinations of gauge invariant loops, such as 2×1 , 2×2 and 3×1 rectangles to systematically remove the higher order in the right-hand side of eq. (2.17). For fermions the improvements consist on actions that preserve certain symmetries more than others, like chiral fermion actions or staggered fermions. On the algorithm side, the currently most used method to generate gauge field configuration is

the Hybrid Monte Carlo method, which combines stochastic sampling with hamiltonian dynamic updates in the gauge field space. Other interesting algorithmic problems regard the calculation of fermion determinants, which typically involve very large sparse matrix diagonalization.

A fundamental concept in Lattice calculations is to recover the continuum limit in a controlled manner at the end of the analysis. The error sources that come into play when discretizing space-time on a fixed lattice are:

- **Finite Volume Effects:** caused by the non infinite domain of the simulation. Usually periodic boundary conditions are implemented to simulate infinite space, but one should always check if the total lattice volume is large enough, especially when dealing with large systems such as multiple baryons.
- **State Isolation and Signal to Noise:** when computing correlators between two points on the lattice it is possible to extract energy states of hadrons by looking at the exponential decay of the correlator in euclidian time. However this problem is largely affect by random noise making it hard to extract even the ground state most of the times; excited states are rarely considered.
- **Chiral Limit:** by which is intended the limit for which the masses of the quarks, and consequently of the computed hadrons, on the lattice approach the physical masses. One might question why this is even the case and that calculations should be performed at the physical masses only. However, the fermion propagator matrix becomes more and more sparse the lower he mass of the quark is, making the numerical algorithms that should diagonalize it slower to converge. The usual approach is to perform calculations on a set of pion masses (this is the usual reference for this problem) and afterwards the limit for $m_{\pi}^{(lat)} \rightarrow m_{\pi}^{(phys)}$ is taken to reproduce the physical observables.
- **Continuum Limit:** perhaps the most obvious thing to do to improve Lattice QCD calculations is to take finer and finer lattice spacings, to approach the continuum case. It should be noted however that this procedure has two downsides. First the lattice spacing in physical units is fixed by the quark masses, and as we previously mentioned, this affects the feasibility of the numerical simulation itself. Secondly, as the lattice approaches the continuum case the autocorrelation of observables in a given ensemble increases rapidly. This behavior, known as “critical slow-down” depends on the observable itself, some are more affected then others The integrated autocorrelatio time for the topological charge for example is believed to have either power-law with a large exponent or even an exponential relation to the lattice spacing.

As one can notice, Lattice QCD is still an open field of research in many aspects: the algorithmic/numerical, the extraction and improvement of the measurement of of observables and the theoretical model itself.

Chapter 3

Advanced Topics in Lattice QCD

In this sections we will present some problems and methods that are used in Lattice QCD and in lattice Pure Gauge Theories. A 4-loop corrected expression for the β -function of QCD will be discussed as well, together with a tentative method of determining the scale parameter Λ from lattice caluclations.

3.1 Scale Setting in the Quenched Approximation

On the lattice quantities are defined to be dimensionless and in order to link them with physical observables they need to be fixed by multiplying them with the lattice spacing a to reproduce the physical units. The fundamental question is then how to connect the lattice spacing to the coupling used in the gluonic action.

In 1993 R. Sommer proposed to use the static quark potential as a reference in the case of $SU(2)$ theory [18]. Later in another work [19] a length scale r_0 was suggested for $SU(3)$ Yang-Mills theory to be set as the distance such that

$$r_0^2 F(r_0) = 1.65 \quad (3.1)$$

with $F(r_0)$ being the force between external static charges. In [19] also a parametrization of the ratio a/r_0 is provided, in terms of the coefficients of the renormalization group equation. To leading order one finds:

$$\frac{a}{r_0} \propto e^{-\frac{\beta}{12b_0}} \quad (3.2)$$

with inverse coupling $\beta = 6/g_0^2$ and b_0 the one loop coefficient of the perturbative expansion of the β function, see section 1.2.1 , $b_0 = 11/(4\pi)^2$. Using the ansatz:

$$\ln \left(\frac{a}{r_0} \right) = \sum_{k=0}^p a_k (\beta - 6)^k \quad (3.3)$$

a parametrization up to $p = 3$ has been fitted to data. The resulting interpolating function is:

$$\ln \left(\frac{a}{r_0} \right) = -1.6805 - 1.7139(\beta - 6) + 0.8155(\beta - 6)^2 - 0.6667(\beta - 6)^3 \quad (3.4)$$

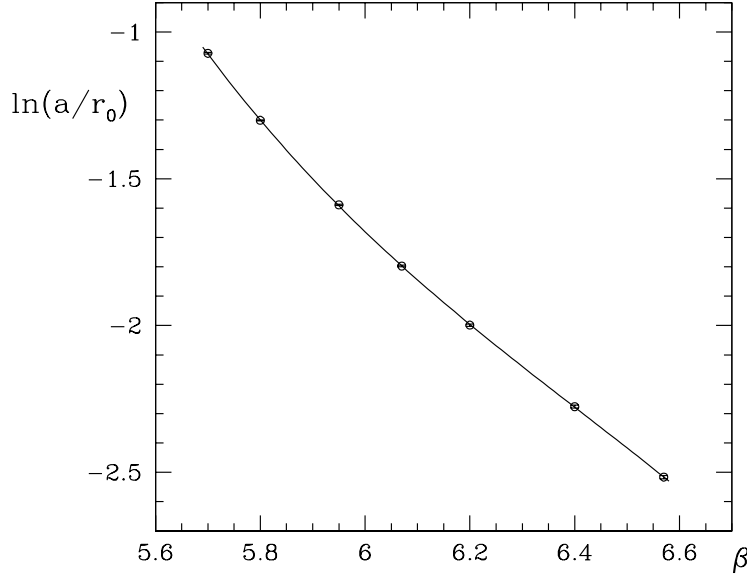


Figure 3.1: Data and interpolating function for $\ln(a/r_0)$ as found in [19].

This scale fixing procedure requires a proper estimate of the length scale from measurements of the static quark potential for various quark sources, which can be an expensive calculation at times. Often it is custom to set the length scale to a fixed value, namely $r_0 = 0.5$ fm, commonly called the Sommer scale parameter, and then use eq. (3.4) to extract a .

More recently another procedure to fix the energy scale has been proposed, based on the Gradient Flow Method, which will be discussed in section 3.3.1. The key idea is again to choose an observable that is lattice spacing independent. By choosing an arbitrary value for it one can use the observable as a reference scale for further calculations.

3.2 The Gradient Flow Method

The Gradient Flow Method, also known as the Wilson Flow in the case of QCD, is a method for studying non-linear quantum field theories by the properties of flows in the field space. The key idea is to see how the theory evolves as it becomes less local, by driving it to the stationary points of the action, applying a “diffusion-like” differential equation to the field in a fictitious dimension called “flow-time”.

For the $SU(3)$ gauge field case most of the theoretical foundation was set by M.Lüscher in [20][21] and for QCD in [22]. Starting from a field $A_\mu(x)$ the characterizing equations are:

$$\begin{aligned}\partial_{t_f} B_\mu &= D_\mu G_{\mu\nu} \\ G_{\mu\nu} &= \partial_\mu B_\nu - \partial_\nu B_\mu + [B_\mu, B_\nu]\end{aligned}\tag{3.5}$$

where the $B(t_f, x)$ field is the flowed version of the original field at flow-time t_f . This is imposed by fixing:

$$B_\mu|_{t_f=0} = A_\mu\tag{3.6}$$

The covariant derivative is extended to represent the derivative of the field B instead of A , this leaves the simple definition for the non-flowed field from the boundary condition. It is generalized straightforwardly as:

$$D_\mu = \partial_\mu + [B_\mu, \cdot] \quad (3.7)$$

In a discretized theory taking the derivatives is not a trivial procedure, but we can use instead the intuitive idea of the flow equations, that is to use the steepest descent method on the action of a field. We then introduce the flowed lattice gauge field $V_{t_f}(x, \mu)$ as the flowed version of a field $U(x, \mu)$. Our flow equation then becomes:

$$\partial_{t_f} V_{t_f}(x, \mu) = -g_0^2 [\partial_{x, \mu} S_G(V_{t_f})] V_{t_f}(x, \mu) \quad (3.8)$$

where S_G is the Wilson action, as defined in eq. (2.19), generalized to flowed fields. The generalization is really straightforward, as it only requires to compute the Wilson loops on the flowed gauge field.

The flow equations for the fermion fields, although they have not been used in this work, are:

$$\begin{aligned} \partial_{t_f} \chi &= \Delta \chi, & \partial_{t_f} \bar{\chi} &= \bar{\chi} \overleftarrow{\Delta} \\ \Delta &= D_\mu D_\mu, & D_\mu &= \partial_\mu + b_\mu \end{aligned} \quad (3.9)$$

note that Δ is the covariant laplacian in this notation. The initial conditions are naturally

$$\chi|_{t_f=0} = \psi, \quad \bar{\chi}|_{t_f=0} = \bar{\psi}, \quad (3.10)$$

3.3 Perturbative Analysis of the Wilson Flow

An important thing to consider when applying the Wilson flow to a field is the renormalization of the observables: one has to check that expectation values of observables at non-zero flow-time are renormalized quantities. Following the calculations performed in [20], we will consider the energy as our base observable.

First, we note that the flow equation is invariant under flow-time independent gauge transformations, this prevents a detailed study of the renormalization. So we consider a modified version of the flow equation by adding one term:

$$\partial_{t_f} B_\mu = D_\mu G_{\mu\nu} + \lambda D_\mu \partial_\nu B_\nu \quad (3.11)$$

the original case is obtained again by setting $\lambda = 0$ and considering:

$$B_\mu = \Lambda B_\mu|_{\lambda=0} \Lambda^{-1} + \Lambda \partial_\mu \Lambda^{-1} \quad (3.12)$$

and with $\Lambda(t, x)$ now being a flow-time dependent gauge transformation, set by:

$$\partial_{t_f} \Lambda_\mu = -\lambda \partial_\nu B_\nu \Lambda \quad \text{with} \quad \Lambda|_{t_f=0} = 1 \quad (3.13)$$

The energy E as defined in eq. (2.36) is a gauge invariant object. One can observe that the modified flow equation is invariant under gauge transformations, hence the energy, as any other gauge invariant observable, will preserve their invariance. Using this modified flow equation it

is possible to write the expectation value of the energy as a function of the flow-time and of the renormalized coupling:

$$\langle E \rangle = \frac{3(N^2 - 1)g_0^2}{128\pi^2 t_f^2} [1 + \bar{c}_1 g_0^2 + \mathcal{O}(g_0^4)] \quad (3.14)$$

with:

$$\bar{c}_1 = \frac{1}{16\pi^2} \left[N \left(\frac{11}{3}L + \frac{52}{9} - 3\ln 3 \right) - N_f \left(\frac{2}{3}L + \frac{4}{9} - \frac{4}{3}\ln 2 \right) \right] \quad (3.15)$$

The equation is for general N , the gauge group dimension, and number of quark flavors N_f . The coefficient \bar{c}_1 is in terms of a scale $L = \ln(8\mu^2 t_f) + \gamma_E$ where μ is the renormalization energy scale and γ_E Euler's constant. From this last relation we can set a flow energy scale as $q = 1/\sqrt{8t_f}$ and give a definition of eq. (3.14) in terms of the running coupling $\alpha_s(q) = \frac{g_0^2}{4\pi}$:

$$\langle E \rangle = \frac{3(N^2 - 1)}{32\pi t_f^2} \alpha_s(q) [1 + k_1 \alpha_s(q) + \mathcal{O}(\alpha_s^2)] \quad (3.16)$$

where the coefficient k_1 is now:

$$k_1 = \frac{1}{4\pi} \left[N \left(\frac{11}{3}\gamma_E + \frac{52}{9} - 3\ln 3 \right) - N_f \left(\frac{2}{3}\gamma_E + \frac{4}{9} - \frac{4}{3}\ln 2 \right) \right] \quad (3.17)$$

In the case of $SU(3)$ symmetry group we have:

$$\langle E \rangle = \frac{3}{4\pi t_f^2} \alpha_s(q) [1 + k_1 \alpha_s(q) + \mathcal{O}(\alpha_s^2)], \quad k_1 = 1.0978 + 0.0075 N_f \quad (3.18)$$

The perturbative expansion is only valid for large values of q , that is when the flow-time is small. We also can notice that $\sqrt{8t_f}$ is the inverse of an energy, or a length. This gives us an intuitive picture of what the gradient flow does, that is to smear the field over a hyper-sphere of radius $\sqrt{8t_f}$. The gradient flow is particularly interesting to study quantities that are divergent on the lattice because of discretization effects, like the topological susceptibility, which become smooth at non-zero t_f . In fig. 3.2 an example of the smearing effect of the gradient flow on the topological charge. The topological charge at $\sqrt{8t_f} = 0$ is highly affected by large fluctuations over the lattice sites. This for example affects the topological susceptibility as it is divergent. One can notice that the action of the flow equation is to remove such low distance fluctuations that at $\sqrt{8t_f} = 0$ fm are almost completely gone. For larger smearing radii the emergence of frozen well separated topological sectors becomes visible.

3.3.1 Scale Fixing with the Gradient Flow

Because of the smearing properties of the flow equation the fields are driven towards the minima of the action, which are in general independent from the lattice spacing. One can therefore set, for sufficiently large flow-times, decide to use the value of $t^2 \langle E \rangle$ to fix the scale of the lattice. This follows naturally from eq. (3.18) as once t^2 is moved to the left hand side only a function of the energy, expressed in terms of $\alpha_s(q)$ remains on the right hand side.

It has been proposed by Lüscher that a value of $t^2 \langle E \rangle = 0.3$ is large enough to be used as a reference scale. In fig. 3.3 we can indeed observe that the value is constant as a function of the lattice spacing (computed instead using the Sommer parameter).

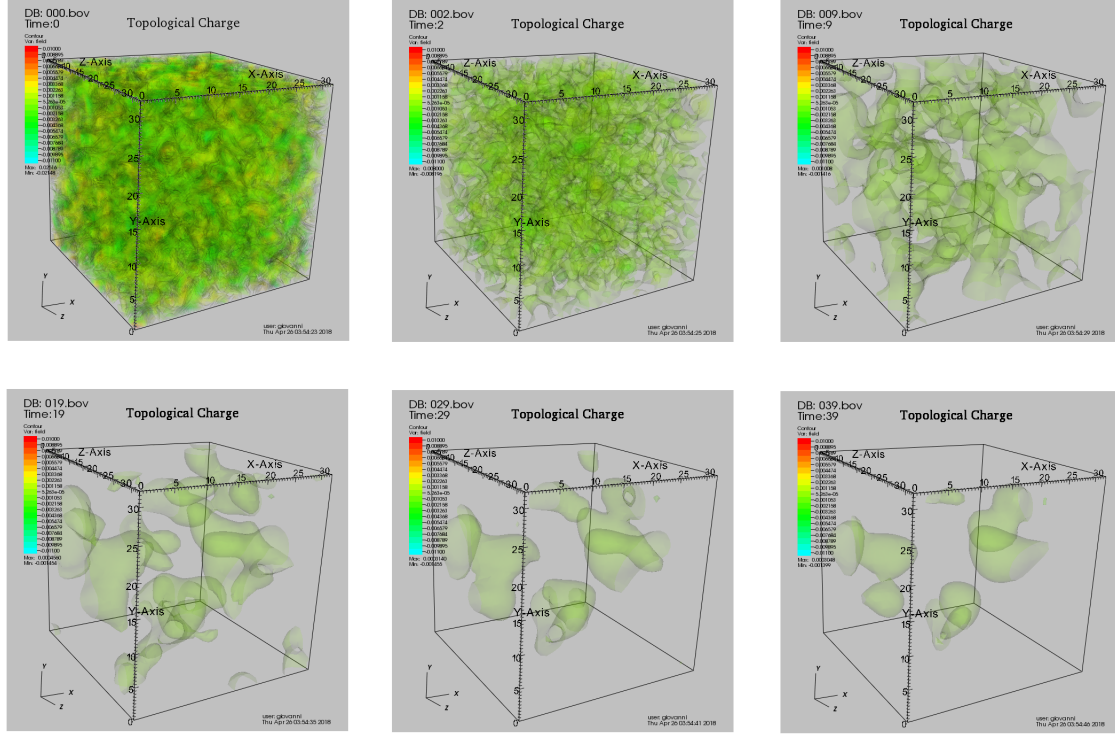


Figure 3.2: Topological charge computed at one euclidean time of a lattice of size $32^3 \times 64$ with lattice spacing 0.06793 fm. The flow different plots are for flow-times $\sqrt{8t_f} = 0, 0.14, 0.30$ fm on the first row and $\sqrt{8t_f} = 0.43, 0.52, 0.60$ fm on the second row.

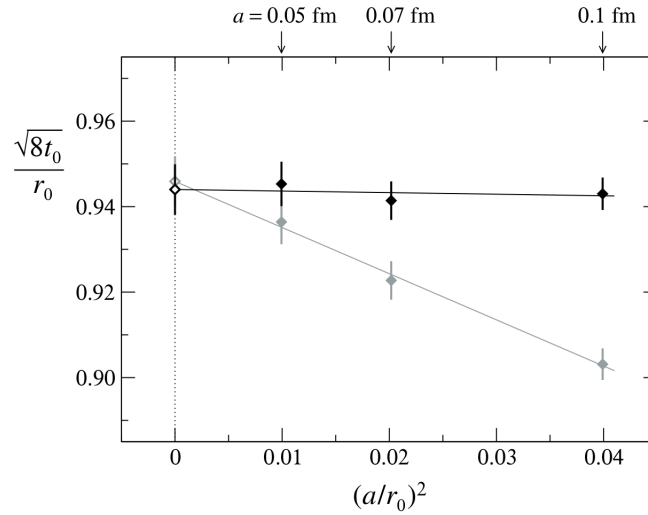


Figure 3.3: Plot of $\sqrt{8t_0}/r_0$ where t_0 is the value such that $t_0^2 \langle E \rangle = 0.3$ for different lattice spacings taken from [23].

3.4 Estimating the Scale Parameter

Finally all the theoretical concepts and tools have been defined to state the main purpose of this work in a formal way. The main goal is to use the perturbative expression of the energy as a function of the flow-time and of the running coupling to estimate the scale parameter Λ . Since the code base that has been developed only for pure gauge theory, we will restrict the analysis for $N_f = 0$ for now, but in a future work the more interesting determination of Λ_{QCD} could be performed the same way.

On the lattice the quantity $t_f^2 \langle E \rangle$ can be computed easily, this leaves only the coupling on the right hand side of eq. (3.18) as the unknown variable. One can then choose an order for the expansion of the Renormalization Group Equation:

$$\mu^2 \frac{d\alpha(\mu)}{d\mu^2} = \beta(\alpha) = -(b_0 \alpha^2 + b_1 \alpha^3 + \dots) \quad (3.19)$$

When solving the equation for $\alpha(\mu)$ there is some freedom on the choice of the renormalization point, as we have seen in eq. (1.17), such that the equation in the end can be simplified by the introduction of a scale parameter.

Using the data computed on the lattice, by first taking the continuum limit in order to account for discretization effects, estimate the scale parameter.

3.4.1 4-loop Corrected Running Coupling

The equation needs to be solved for $\alpha(\mu)$ and a convenient approximate form, correct up to order 4, that is including 4-loop diagrams in the calculations, parametrized by 4 coefficients can be found in [24]:

$$\alpha(\mu) = \frac{1}{b_0 t} \left[1 - \frac{b_1 \ln t}{b_0 t} + \frac{b_1^2 (\ln^2 t - \ln t - 1) + b_0 b_2}{b_0^4 t^2} - \frac{b_1^3 (\ln^3 t - \frac{5}{2} \ln^2 t - 2 \ln t + \frac{1}{2}) + 3b_0 b_1 b_2 \ln t - \frac{1}{2} b_0^2 b_3}{b_0^6 t^3} \right] \quad (3.20)$$

there the convenient notation of $t \equiv \ln \frac{\mu^2}{\Lambda^2}$ has been introduced. The coefficients b_0, b_1, b_2 and b_3 can be computed analytically for a general theory on $SU(3)$ with N_f quark flavors. While b_0 and b_1 have known exact values, the other two parameters are renormalization scheme dependent,

and we chose the ones computed in the \overline{MS} found in [25]. The coefficients are then:

$$\begin{aligned}
 b_0 &= \frac{1}{(4\pi)} \left[11 - \frac{2}{3}N_f \right] \\
 b_1 &= \frac{1}{(4\pi)^2} \left[102 - \frac{38}{3}N_f \right] \\
 b_2 &= \frac{1}{(4\pi)^3} \left[\frac{2857}{2} - \frac{5033}{18}N_f + \frac{325}{54}N_f^2 \right] \\
 b_3 &= \frac{1}{(4\pi)^4} \left[\left(\frac{149753}{6} + 3564\zeta_3 \right) - \left(\frac{1078361}{162} + \frac{6508}{27}\zeta_3 \right) N_f \right. \\
 &\quad \left. + \left(\frac{50065}{162} + \frac{6472}{81}\zeta_3 \right) N_f^2 + \frac{1093}{729}N_f^3 \right]
 \end{aligned} \tag{3.21}$$

or in a numerical form, substituting also the Reiemann zeta-funtion value $\zeta_3 = 1.202056903 \dots$ one gets the more handy expression

$$\begin{aligned}
 b_0 &\approx \frac{1}{(4\pi)} (11 - 0.66667N_f) \\
 b_1 &\approx \frac{1}{(4\pi)^2} (102 - 12.6667N_f) \\
 b_2 &\approx \frac{1}{(4\pi)^3} (1428.50 - 279.611N_f + 6.01852N_f^2) \\
 b_3 &\approx \frac{1}{(4\pi)^4} (29243.0 - 6946.30N_f + 405.089N_f^2 + 1.49931N_f^3)
 \end{aligned} \tag{3.22}$$

with the aid of these coefficients the only unknown variable in eq. (1.17) is the scale parameter, so by fitting this function to the lattice over a range of energies where some degree of overlap is found leads to an estimation of Λ .

Part II

Implementation

Chapter 4

Designing a Lattice $SU(3)$ Yang-Mills Theory Code

One of the major focuses of this work has been a completely new implementation of a program to generate and analyze $SU(3)$ gauge fields. As it is common practice in Lattice QCD numerical implementations, the program is separated in two parts that are computationally intensive and one that is easier in that sense:

- *generation of gauge fields*: in this case it is done through a simple Metropolis algorithm using the standard Wilson action;
- *computation of observables*: this includes applying the gradient flow as well as computing the energy density and the topological charge at every flow-time;
- *computation of derived observables*: mainly post analysis, error analysis and model fits to data.

Here we will present the main features of the first two steps, which are the most interesting ones. The programming language of choice is `C++` because of its high efficiency, high abstraction capabilities (the code-base is highly object oriented) and for the easiness of the `MPI` integration. The analysis of data has been performed using `python` and in particular relying heavily on its standard data science packages such as `numpy` and `pandas`.

4.1 Generating Pure Gauge Fields

The task of generating lattice field configurations is extremely demanding in terms of computation requirements. The case of QCD is much more demanding than that of a pure Yang-mills theory, but overall the latter calculation is still challenging. The main, and perhaps overwhelmingly simple, reason for this problem is the dimensionality. Dealing with a discretized space-time

lattice, things tend to scale with powers of 2^4 , a trivial example is cutting in half the lattice spacing keeping a fixed total volume: this requires 16 more points in the global lattice.

To get a better feeling of the algorithm we first have to look at what the basic object of the program is: the lattice. The number of double precision floating point numbers to be stored for a field configuration is given by

$$\underbrace{N^3}_{\text{spatial dimension}} \times \underbrace{N_t}_{\text{time dimension}} \times \underbrace{4}_{\text{links per site}} \times \underbrace{9}_{\text{SU(3) matrix size}} \times \underbrace{2}_{\text{real and imaginary part}} \quad (4.1)$$

this implies that, for example, if we choose $N = 48$, $N_t = 96$ the resulting configuration is 6115295232 *bytes* large, that is 5.7 *GBytes*. This limits greatly the possibility of simulating large systems

The basic element at each lattice site is a set of 4 different $SU(3)$ matrices, one for each dimension. These links are to be intended as the integral of the gauge field from one site to the adjacent one along each dimension. A more formal description has been given in chapter 3.

4.1.1 The Metropolis Algorithm

The main algorithm that has been used to generate an ensemble of gauge field configurations is the Metropolis Algorithm. It is a widely popular Markov Chain Monte Carlo Method to generate a sequence of random samples from a probability distribution [26].

In general, a Markov Chain is a sequence randomly chosen variables X_1, X_2, \dots, X_t , in our case a lattice field configuration, with the Markov Property: that is the probability of the step $t + 1$ depends only on the variable X_t :

$$P(X_{t+1} = x | X_1 = x_1, X_2 = x_2, \dots, X_t = x_t) = P(X_{t+1} = x | X_t = x_t) \quad (4.2)$$

In the case where the probabilities of moving from a state $X_i = i$ to a state $X_j = j$ is not known, the transition probability from the two states, $W(i \rightarrow j)$ can be split into two contributions: the probability $T(i \rightarrow j)$ for making the transition to state j being in state i and the probability of accepting this transition $A(i \rightarrow j)$.

$$W(i \rightarrow j) = A(i \rightarrow j)T(i \rightarrow j) \quad (4.3)$$

if a Probability Distribution Function (PDF) is known for the process, we can label the probability of a given state at a fixed time $w_i(t)$. The transition probability to a state j at time $t + 1$ is the sum of the transition probabilities of moving to state j from state i plus the probability of being in state i at time t and rejecting to move to any other state:

$$\begin{aligned} w_j(t+1) &= \sum_i [w_i(t)T(i \rightarrow j)A(i \rightarrow j) + w_j(t)T(j \rightarrow i)(1 - A(j \rightarrow i))] \\ &= w_j(t) + \sum_i [w_i(t)T(i \rightarrow j)A(i \rightarrow j) - w_j(t)T(j \rightarrow i)A(j \rightarrow i)] \end{aligned} \quad (4.4)$$

for large t , when the equilibrium is reached, we require that $w_j(t+1) = w_j(t) = w_j$, and thus we have:

$$\sum_i w_i T(i \rightarrow j) A(i \rightarrow j) = \sum_i w_j T(j \rightarrow i) A(j \rightarrow i) \quad (4.5)$$

now, considering that the transition probability from a state j to all other states must be normalized $\sum_i W(j \rightarrow i) = \sum_i T(j \rightarrow i)A(j \rightarrow i) = 1$ we get:

$$\sum_i w_i T(i \rightarrow j) A(i \rightarrow j) = w_j \quad (4.6)$$

At this point, the further constrain of Detailed Balance is introduced, that is:

$$w_i W(i \rightarrow j) = w_j W(j \rightarrow i) \quad (4.7)$$

at equilibrium we then have:

$$\frac{w_i}{w_j} = \frac{W(i \rightarrow j)}{W(j \rightarrow i)} = \frac{T(i \rightarrow j)A(i \rightarrow j)}{T(j \rightarrow i)A(j \rightarrow i)} \quad (4.8)$$

Making the approximation that the transition probability between states is the same, $T(i \rightarrow j) = T(j \rightarrow i)$, the brute-force approach, we are left with the acceptance ratio of a move to

In our case the probability distribution is the exponential of gluon Wilson Action, as we can see from (REFLINK NEEDED), and our random samples are the gauge configurations themselves. A simplified version of the algorithm is described below:

Algorithm 1 Metropolis Algorithm

- 1: *configuration* \leftarrow initial configuration
 - 2: **for** $i < MonteCarloCycles$ **do**
 - 3: *newConfiguration* \leftarrow random move + *configuration*
 - 4: $\Delta S \leftarrow \text{action}(\text{newConfiguration}) - \text{action}(\text{configuration})$
 - 5: **if** $\Delta S > \text{random}(0, 1)$ **then**
 - 6: *configuration* \leftarrow *newConfiguration*
-

The actual implementation of this algorithm on a lattice is however not as trivial as it seems, because we are dealing with a lattice gauge configuration, so we need to define what is a random move and what is the action difference for our specific case.

One configuration is saved, in the form of a simple binary containing all the data of the lattice, as an intermediate result every N_C Monte Carlo updates. We need this in order to apply the gradient flow afterwards to the configurations and compute the observables we want. The choice of N_C turned out to be crucial for the autocorrelation of some observables, in particular the topological charge.

4.1.2 Sampling the Configuration Space

To use Metropolis' algorithm we need to define what a random move is. Using the Wilson Action eq. (2.11), which is defined on plaquettes, an update on a single link variable can be seen as a small unitary transformation. In order to generate such transformation use three random $SU(2)$ matrices "close to unity". By this expression we mean that the real diagonal

components are the dominant terms of the matrix. A recipe for generating these matrices is found in [12].

$$R_2 = \begin{pmatrix} r_{11} & r_{12} \\ r_{21} & r_{22} \end{pmatrix} \quad S_2 = \begin{pmatrix} s_{11} & s_{12} \\ s_{21} & s_{22} \end{pmatrix} \quad T_2 = \begin{pmatrix} t_{11} & t_{12} \\ t_{21} & t_{22} \end{pmatrix} \quad (4.9)$$

The elements of the matrix are chosen at random by choosing four random numbers r_0, \mathbf{r} (a three component vector) between $(-\frac{1}{2}, \frac{1}{2})$. We then introduce a "spread parameter" ϵ that controls how much the off-diagonal terms will weight, so we scale our random variables by:

$$x_0 = \text{sign}(r_0)\sqrt{1 - \epsilon^2} \quad \mathbf{x} = \epsilon \frac{\mathbf{r}}{|\mathbf{r}|} \quad (4.10)$$

and we use these coefficients together with the generators of the $SU(2)$ group (the Pauli matrices) to build an element of the group:

$$U = x_0 \mathbf{1} + i\mathbf{x} \cdot \boldsymbol{\sigma} = \begin{pmatrix} u_{11} & u_{12} \\ u_{21} & u_{22} \end{pmatrix} \quad (4.11)$$

We then embed these $SU(2)$ matrices in three $SU(3)$ matrices by mapping them as:

$$R = \begin{pmatrix} r_{11} & r_{12} & 0 \\ r_{21} & r_{22} & 0 \\ 0 & 0 & 1 \end{pmatrix} \quad S = \begin{pmatrix} s_{11} & 0 & s_{12} \\ 0 & 1 & 0 \\ s_{21} & 0 & s_{22} \end{pmatrix} \quad T = \begin{pmatrix} 1 & 0 & 0 \\ 0 & t_{11} & t_{12} \\ 0 & t_{21} & t_{22} \end{pmatrix} \quad (4.12)$$

These three matrices are clearly members of $SU(3)$ and so is their product $X = RST$. We thus have defined a recipe for numerically generating random group transformations, the key element for our algorithm.

An additional element that we need to define is the action difference ΔS . On a single link $U_\mu(x)$ we apply a random transformation X and get $U'_\mu(x) = XU_\mu(x)$. The total change in the action only depends on those plaquettes that contain the considered link variable. In four dimensions there are 12 such elements:

$$\Delta S = S[U'_\mu(x)] - S[U_\mu(x)] = -\frac{\beta}{N} \Re \text{Tr}[U'_\mu(x) - U_\mu(x)]A \quad (4.13)$$

where A is the sum of the "staples" of the link U . They are the constant three sides of the plaquettes that contain U :

$$A = \sum_{\nu \neq \mu} \left[U_\nu(x + \mu) U_{-\mu}(x + \mu + \nu) U_{-\nu}(x + \nu) \right. \\ \left. + U_{-\nu}(x + \mu) U_{-\mu}(x + \mu - \nu) U_\nu(x - \nu) \right] \quad (4.14)$$

$$S[U_\mu] = \sum_{\nu \neq \mu} \left(\begin{array}{c} \text{square loop} \\ + \\ \text{rectangle loop} \end{array} \right) = \longrightarrow \times \sum_{\nu \neq \mu} \left(\begin{array}{c} \text{staple loop} \\ + \\ \text{another staple loop} \end{array} \right)$$

Figure 4.1: Schematic representation of the symmetric definition of action $S[U_\mu]$ expressed as a function of the staples .

Algorithm 2 Metropolis Update

```

1: for  $x, \mu$  do
2:    $A \leftarrow \text{computeStaples}(x, \mu)$ 
3:   for  $i < N_H$  do
4:      $U_{\text{new}}(x, \mu) \leftarrow X \cdot U(x, \mu)$ 
5:      $\Delta S \leftarrow (U_{\text{new}}(x, \mu) - U(x, \mu)) \cdot A$ 
6:     if  $\text{realTrace}(\Delta S) > \text{random}(0, 1)$  then
7:        $U(x, \mu) \leftarrow U_{\text{new}}(x, \mu)$ 

```

4.1.3 Updates Strategies

There is now some arbitrariness in what is defined as an update. In this work we call an update the following procedure:

These updates are the ones we consider when we refer to Monte Carlo cycles, autocorrelation times and so on. Note that each update includes a loop over all links on the lattice and that every link is "hit" N_H times before moving to the next one. This is done for computational efficiency, because computing the staples is the most expensive part of the algorithm, once A is computed for a link, the result is used to attempt multiple updates on the link. It can also be shown that if N_H is sufficiently large the algorithm becomes equivalent to the heatbath algorithm.

The order in which the links in the lattice are visited is also arbitrary. The simplest way, the ordered one, was adopted. This however might have impacted the autocorrelation of the system, not allowing significant modification to the system as an update depends on the neighbors. An alternative choice is a checkerboard pattern, which has potential benefits to the autocorrelation time of the observables as well as on the parallelization scheme ??.

4.1.4 Parallelization Scheme

Given the size of the lattice (from $V \approx 10^5$ to $V \approx 10^7$, the total number of lattice sites), it is necessary to split the computation of the updates on more than one processors. The most direct way is to divide the lattice into sub-blocks and have each process handle its portion of the field alone.

FIG: blocks?

However, because of the dependence of the action difference of a link on its neighbors, when updating a link on the edge of a sub-block information about another block is needed. Here is where the Message Passing Interface (MPI) comes in use. For this particular problem we decided to use a point to point communication scheme between the processors, the use of periodic boundary conditions allowed also for non-blocking communications to be used, in particular the collective geometry based scheme shown in fig. ?? has been implemented.

FIG: sendrecv

Note that the communication is relevant only for the computation of the staples, this is another argument in favor of performing multiple hits on a link at every update. It is clear to see that the algorithm can be affected by large communication overhead problems. If the sub-blocks are too small, then most of the time would be spent on sending and receiving links from the neighbors. This causes the execution time to depend not linearly on the number of processors, instead the relation flattens at some value given by the communication overhead.

4.1.5 Summary of the Parameters

In total the algorithm need four parameters as inputs. Of these, only one defines the physics of the system, the others have to be set and optimized in order to improve the acceptance ratio of the metropolis test and the autocorrelation of the observables computed on the generated configurations.

Parameter	Description
β	Coupling parameter of the Wilson Action
ϵ	"Spread" of the random $SU(3)$ elements for the updates
N_C	Number of updates between one saved configuration (observable measurement)
N_H	Number of of "hits" per link at every update, with constant staple

Table 4.1: Parameters for the Monte Carlo generation of Yang-Mills gauge field configurations via the Metropolis Algorithm

4.2 Wilson Flow of Gauge Configurations

To study the flow-time dependence of the observables a numeric implementation of eq. (3.8) is needed. The main challenge that this problem poses is how to numerically integrate the flow equation on the lattice, because it is important to preserve the $SU(3)$ Lie Group structure of the field through the numerical procedure. The problem is solved by using the so called Structure-Preserving Runge-Kutta Methods, in particular the Runge-Kutta Munthe-Kaas method that is designed to integrate first order ODE on a manifold [27, 28, 29]. The problem can be defined

in a more general manner as:

$$\dot{V}_t = Z(V_t)V_t \quad (4.15)$$

here V_t is an element of a Lie group \mathcal{G} and $Z(V_t)$ is a function with values in the associated algebra \mathfrak{g} . The general ansatz for the RKMK method is to write the integration step, with ϵ the integration step, as:

$$V_{t+\epsilon} = \exp[\epsilon\Omega(V_t)]V_t \quad (4.16)$$

where $\Omega(V_t)$ is a linear combination of $Z(V_t + \epsilon c_i)$, with c_i the RK coefficients, and of their commutators. Following the suggestion of [20] and considering the analysis of [30] that suggests that, for a fixed step size, an integrator of third order is sufficient. The integration scheme that has been used is the one found in Lüscher's article:

$$\begin{aligned} W_0 &= V_t \\ W_1 &= \exp\left[\frac{1}{4}Z_0\right] W_0 \\ W_2 &= \exp\left[\frac{8}{9}Z_1 - \frac{17}{36}Z_0\right] W_1 \\ V_{t+\epsilon} &= \exp\left[\frac{3}{4}Z_2 - \frac{8}{9}Z_1 + \frac{17}{36}Z_0\right] W_2 \end{aligned} \quad (4.17)$$

where the shorthand notation $Z_i = \epsilon Z(W_i)$ has been introduced. The choice of the coefficients for the Butcher's tableau of the RK method is made in order to satisfy the requirements for a third order RK integrator and to cancel the commutator terms in $\Omega(V_t)$.

What is then left to define are the derivative of the action at a given lattice site and the numerical exponentiation of an $\mathfrak{su}(3)$ element, which returns an $SU(3)$ element.

4.2.1 The Action Derivative

Following the procedure in [31] we define the derivative of the action at a lattice site $U_\mu(x)$ to be:

$$\partial_\mu S[U_\mu(x)] = \frac{i}{2} \left(\Omega_\mu(x) - \frac{1}{3} \mathbb{1} \Im \text{Tr}[\Omega_\mu(x)] \right) \quad (4.18)$$

with

$$\Omega_\mu(x) = U_\mu(x)A_\mu(x) - A_\mu^\dagger(x)U_\mu^\dagger(x) \quad (4.19)$$

where $A_\mu(x)$ are the staples of the link. We can note that the derivative is always traceless hermitean matrix, thus an element of $\mathfrak{su}(3)$ as expected.

4.2.2 Exponential of a $\mathfrak{su}(3)$ Element

Again following [31] we provide a numerical recipe for taking the exponential function of a traceless hermitean 3×3 matrix. The key idea is to use the Cayley-Hamilton theorem, that states that every matrix is a zero of its characteristic polynomial:

$$Q^3 - c_1 Q - c_0 \mathbb{1} = 0, \quad \text{with } c_0 = \det Q = \frac{1}{3}(Q^3), \quad c_1 = \frac{1}{2}(Q^2) \quad (4.20)$$

The exponential of iQ can then be written as:

$$e^{iQ} = f_0 \mathbb{1} + f_1 Q + f_2 Q^2 \quad (4.21)$$

where the functions of the eigenvalues of Q , which in turn can be parameterized, because of the hermitianity of Q in terms of c_0 and c_1 . Labeling the eigenvalues of Q as q_1, q_2, q_3 and using the fact that the matrix is traceless they can be parametrized as:

$$q_1 = 2u \quad q_2 = -u + w \quad q_3 = -u - w \quad (4.22)$$

with:

$$u = \sqrt{\frac{1}{3}c_1} \cos\left(\frac{1}{3}\theta\right) \quad w = \sqrt{c_1} \sin\left(\frac{1}{3}\theta\right) \quad \theta = \arccos\left[\frac{c_0}{2} \left(\frac{3}{c_1}\right)^{3/2}\right] \quad (4.23)$$

As shown in [31] the coefficients f_i can be written as:

$$f_i = \frac{h_i}{9u^2 - w^2} \quad (4.24)$$

with:

$$\begin{aligned} h_0 &= (u^2 - w^2)e^{2iu} + e^{-iu} \left[8u^2 \cos(w) + 2iu(3u^2 + w^2) \frac{\sin(w)}{w} \right] \\ h_1 &= 2ue^{2iu} - e^{-iu} \left[2u \cos(w) - i(3u^2 - w^2) \right] \\ h_2 &= e^{2iu} - e^{-iu} \left[\cos(w) + 3iu \frac{\sin(w)}{w} \right] \end{aligned} \quad (4.25)$$

This fairly complicated algorithm is the core of the gradient flow implementation, because fundamentally the integration of the flow equation is a series of matrix exponentials over every action derivative of the lattice.

4.2.3 Parallelization Scheme

Also this problem is very expensive in computational terms, so it is worth designing a parallelization scheme for it. The idea is still to split the lattice into sub-blocks and have each processor handle one of them. By looking at eq. (4.17) we see that all operations can be defined on a lattice-wise scale and that they all depend on one previous state of the field, not on an intermediate one as was the case for the generation of gauge fields. This allows us to define a "shift" operation, that effectively creates an additional lattice that is the translation of the original along an axis. The huge advantage is that in order to perform this operation only one communication instance is needed (following the previous scheme in section 4.1.4), but the message is now a whole shared cube between to processors.

FIG: cubes being shared ADD ALGO...

This has to be implemented for the action derivative lattice and the gauge field itself. The massive reduction in communication overhead improves the scaling of the algorithm greatly, making this part of the problem much more efficient.

4.3 Structure and Tools

The full code can be found on the web under the link [github...](#) , where both the code for the generation and the flow of gauge fields is hosted. The technical documentation is found at [documentation...](#) . As already mentioned the language of choice was C++, mainly because of the high-performance and abstraction level it provides. An object-oriented structure has been used, as can be seen in [FIG: scheme class](#) . Notable tools that have been used that deserve a mention are MPI, nlhoman json (used for easy input parameters handling via json files), cmake (for building the project) and valgrind for function and memory profiling.

Chapter 5

Tests and Runs Description

5.1 Generated Ensembles

In order to study the scale parameter in the continuum limit, it has been necessary to choose a set of decreasing lattice spacings to then be able to take the continuum limit. The lattice spacing is linked to the coupling g and β by the known relation: **SOMMER E LOG** We chose 4 values of β that span lattice spacings from approximately 0.1 fm to 0.05 fm in approximately equal steps.

For the calculation to be consistent however, the total volume of the lattice should be kept constant, so the choice of the lattice spacings also determined the number of lattice sites per dimension, having $L = aN \approx \text{const.}$ The time dimension has been take to be twice as big as the space dimension.

Table **(REFLINK NEEDED)** summarizes the physical properties of the ensembles that were generated. For each value of β a statistical ensemble was needed. Ideally, one would take

β	a	$N^3 \times T$	aL [fm]
6.00	0.98	$24^3 \times 48$	2.2
6.10	0.98	$28^3 \times 56$	2.2
6.20	0.98	$32^3 \times 64$	2.2
6.45	0.98	$48^3 \times 96$	2.2

Table 5.1: Physical properties of the ensembles used for this work.

as many configurations as possible for each value and in principle one would have the same number of configurations for each of them. However it is clear from the discussion in chapter **(REFLINK NEEDED)** that the number of lattice sites affects computation times and the capability of storing the configurations dramatically. Moreover, as we will discuss in chapter **(CITATION NEEDED)** the autocorrelation time of the observables has a non-trivial, power-law or exponential, behavior with the lattice spacing, making the generation of the larger β ensembles even more time consuming.

autocorr for topc at different beta The following table summarizes the final values for the pa-

rameters of the Metropolis algorithm for the different ensembles. These values have been chosen

β	N_{conf}	N_{corr}	MC Steps	N_{hit}
6.0	1000	200	200000	30

Table 5.2: Physical properties of the ensembles used for this work.

after many tests, checks of the autocorrelation time and mainly in an empirical way. There are some parameters that are free in principle and no real reference study on their impact on the resulting ensemble. In the next section the trial and error approach that led to this decision will be briefly discussed.

5.2 Test Runs

Running some test calculations with a completely new code base is obviously necessary. First some benchmarks to check the expectation values of the observables, both on raw configurations as on flowed configurations. These benchmarks were made using 2 configurations generated with the CHROMA (CITATION NEEDED) code base from USQCD for zero flow-time observables and one configuration flowed using an extension of CHROMA called FlowOps (CITATION NEEDED), built on QDP++, that applies the Wilson flow to configurations. Both types of test, once all the parameters were made equal, gave results equal to machine precision with the ones generated with the new code base.

Checking the validity of expectation values of observables is a solid indication that the overall back-end of the new code-base has been implemented well, as the results are deterministic. Testing the Metropolis algorithm and assessing the quality of the generated ensembles is much harder, because it involves stochastic computations, hence no numerical check can be easily defined, one can only look at average properties of the ensemble. Unfortunately the generation of gauge field configuration as we saw in (REFLINK NEEDED) TABLE has 3 parameters that need to be set that do affect the statistical properties of the ensemble, mainly the autocorrelation.

5.2.1 Strong and Weak Scaling

First we can look at the scaling properties of the two sections of the code. We will distinguish the analysis in the two usual quantities used in High Performance Computing for parallel programs: strong and weak scaling.

Strong scaling is the performance of a program measured in execution time as a function of the number of processors used. One would obviously expect the relation to be ideally inverse, with execution time dropping as $1/N_{procs}$, however given the overhead caused by parallelization this is seldomly the case.

Weak scaling is the measure of the performance of a program as the size of the system increases but by keeping the total workload assigned to each processor constant. This measure is

important to assess the quality of the parallelization scheme as it gives insights on how much time is spent in communication as more inter-processor messages are being sent. **FIG: PLOT SCALING COMMENTI...**

5.2.2 Autocorrelation of Observables

The most important test has been the assessment of the autocorrelation time for different observables at various lattice spacings varying the parameters of the generation algorithm. The first test shows the integrated autocorrelation time for **asdasd** at fixed N_{corr} for different lattice spacings:

FIG: PLOT autocorr spacing COMMENTI...

Next we looked at a single lattice spacing and tried to vary the parameters N_{corr} and N_{hits} . The choice of the lattice spacing, motivated by the previous analysis, has been $\beta = 6.45$.

FIG: PLOT autocorr params COMMENTI...

5.3 Production Runs and Timing

All production runs were carried out on the High Performance Computing Center at Michigan State University (MSU), with the support of the Institute for Cyber-Enabled Research (iCER). Development was performed on local machines and on the small cluster SMAUG located at the Department of Physics of the University of Oslo (UiO) and some larger benchmarks were run on the Abel Computer Cluster also at UiO.

The final ensembles were generated using the parameters in table **(REFLINK NEEDED)**, shows the computing resources used for the generation of all four ensembles.

Part III

Data Analysis and Results

Chapter 6

Raw Observables

Chapter 7

Running Coupling and Scale Fixing

Part IV

Conclusion and Discussion

Chapter 8

Summary and Conclusion

Chapter 9

Future Developements

Part V

Appendices

Bibliography

- [1] UX: Standard model of the standard model.
- [2] Schroder Peskin. *An Introduction to Quantum Field Theory*. Cambridge University Press, 1989.
- [3] Shahida Dar. The neutron EDM in the SM : A review.
- [4] A Chaudhuri. A short course on relativistic heavy ion collisions. 07 2012.
- [5] G Dissertori. 9. QUANTUM CHROMODYNAMICS. page 50.
- [6] David J. Gross and Frank Wilczek. Ultraviolet behavior of non-abelian gauge theories. *Phys. Rev. Lett.*, 30:1343–1346, Jun 1973.
- [7] H. David Politzer. Reliable perturbative results for strong interactions? *Phys. Rev. Lett.*, 30:1346–1349, Jun 1973.
- [8] A Dainese, E Scomparin, G Usai, P Antonioli, R Arnaldi, Andrea Beraudo, E Bruna, G E. Bruno, S Bufalino, P Di Nezza, M Lombardo, R Nania, F Noferini, C Oppedisano, S Piano, F Prino, Alessandro Rossi, Michelangelo Agnello, Wanda Alberico, and C Zampolli. INFN what next: Ultra-relativistic heavy-ion collisions.
- [9] R Machleidt and F Sammarruca. Chiral EFT based nuclear forces: achievements and challenges. 91(8):083007.
- [10] S.K. Bogner, R.J. Furnstahl, and A. Schwenk. From low-momentum interactions to nuclear structure. 65(1):94–147.
- [11] Kenneth G. Wilson. Confinement of quarks. 10(8):2445–2459.
- [12] Christof Gattringer and Christian B. Lang. *Quantum Chromodynamics on the Lattice*, volume 788 of *Lecture Notes in Physics*. Springer Berlin Heidelberg.
- [13] Rajan Gupta. Introduction to lattice QCD.
- [14] E. Witten. Current algebra theorems for the $u(1)$ goldstone boson. 156(2):269–283.
- [15] Adriano Di Giacomo. Topology in lattice QCD.

- [16] Constantia Alexandrou, Andreas Athenodorou, Krzysztof Cichy, Arthur Dromard, Elena Garcia-Ramos, Karl Jansen, Urs Wenger, and Falk Zimmermann. Comparison of topological charge definitions in lattice QCD.
- [17] David J. Gross, Robert D. Pisarski, and Laurence G. Yaffe. QCD and instantons at finite temperature. 53(1):43–80.
- [18] R. Sommer. A new way to set the energy scale in lattice gauge theories and its application to the static force and α_s in SU(2) yang–mills theory. 411(2):839–854.
- [19] M. Guagnelli, R. Sommer, and H. Wittig. Precision computation of a low-energy reference scale in quenched lattice QCD. 535(1):389–402.
- [20] Martin Lscher. Properties and uses of the wilson flow in lattice QCD. 2010(8).
- [21] Martin Lscher and Peter Weisz. Perturbative analysis of the gradient flow in non-abelian gauge theories. 2011(2).
- [22] Martin Lscher. Chiral symmetry and the yang–mills gradient flow. 2013(4).
- [23] Martin Lscher. Erratum: Properties and uses of the wilson flow in lattice QCD. 2014(3).
- [24] G Dissertori. 9. QUANTUM CHROMODYNAMICS. page 50.
- [25] T. van Ritbergen, J. A. M. Vermaseren, and S. A. Larin. The four-loop beta-function in quantum chromodynamics. 400(3):379–384.
- [26] Nicholas Metropolis, Arianna W. Rosenbluth, Marshall N. Rosenbluth, Augusta H. Teller, and Edward Teller. Equation of state calculations by fast computing machines. 21(6):1087–1092.
- [27] Hans Munthe-Kaas. Runge-kutta methods on lie groups. 38(1):92–111.
- [28] Hans Munthe-Kaas. Lie-butcher theory for runge-kutta methods. 35(4):572–587.
- [29] Elena Celledoni, Hkon Marthinsen, and Brynjulf Owren. An introduction to lie group integrators basics, new developments and applications. 257:1040–1061.
- [30] Marco C, Cristian Consonni, Georg P. Engel, and Leonardo Giusti. Non-gaussianities in the topological charge distribution of the SU(3) yang–mills theory. 92(7).
- [31] Colin Morningstar and Mike Peardon. Analytic smearing of SU (3) link variables in lattice QCD. 69(5).